

AIAA
39p.

NB
P.①

MOLECULAR PROCESSES IN COMETS

Grant NSG-7421

7N-90

Semiannual Progress Report No. 13

29604

For the period 1 January through 30 June 1984

Principal Investigator
Dr. A. Dalgarno

RECEIVED
AIAA
1984 AUG 22 AM 9:19
I.I.S. LIBRARY

Prepared for

National Aeronautics and Space Administration
Washington, D. C. 20546

July 1984

Smithsonian Institution
Astrophysical Observatory
Cambridge, Massachusetts 02138

The Smithsonian Astrophysical Observatory
is a member of the
Harvard-Smithsonian Center for Astrophysics

The NASA Technical Officer for this grant is Dr. H. C. Brinton, Code EL-4,
Sl/Planetary Programs, NASA, Washington, D. C. 20546

MOLECULAR PROCESSES IN COMETS

Grant NSG-7421

Semiannual Progress Report No. 13

For the period 1 January through 30 June 1984

Principal Investigator
Dr. A. Dalgarno

Prepared for

National Aeronautics and Space Administration
Washington, D. C. 20546

July 1984

Smithsonian Institution
Astrophysical Observatory
Cambridge, Massachusetts 02138

The Smithsonian Astrophysical Observatory
is a member of the
Harvard-Smithsonian Center for Astrophysics

The NASA Technical Officer for this grant is Dr. H. C. Brinton, Code EL-4,
S1/Planetary Programs, NASA, Washington, D. C. 20546

MOLECULAR PROCESSES IN COMETS

Grant NSG-7421

Semianual Progress Report No. 13

For the period 1 January - 30 June 1, 1984

Principal Investigator

Dr. A. Dalgarno

The paper on the photodissociation of cometary OH and OD has been accepted for publication in Icarus. For that work, it became necessary to develop a multichannel theory of photodissociation to take proper account of the contribution from the $2^2\Pi$ and $3^2\Pi$ states which are strongly mixed by radial coupling. A preprint of the work is attached. We are now exploring the situation regarding the cometary molecules CO and CH.

CENTER FOR ASTROPHYSICS

PREPRINT SERIES

No. 2001

RESONANCES IN THE PHOTODISSOCIATION OF OH BY ABSORPTION INTO COUPLED $^2\Pi$ STATES: ADIABATIC AND DIABATIC FORMULATIONS

Ewine F. van Dishoeck
Sterrewacht Leiden, Huygens Laboratorium, The Netherlands

Marc C. van Hemert

Department of Physical and Macromolecular Chemistry, Gorlaeus Laboratories, The Netherlands

A.C. Allison

Harvard-Smithsonian Center for Astrophysics
and

Department of Computing Science, The University, Glasgow, Scotland
and

A. Dalgarno

Harvard-Smithsonian Center for Astrophysics

Submitted to

Journal of Chemical Physics

Center for Astrophysics

60 Garden St.

Cambridge, Massachusetts 02138

Harvard College Observatory

Smithsonian Astrophysical Observatory

Abstract. The bound $3^2\Pi$ and repulsive $2^2\Pi$ states of OH are strongly coupled by the action of the nuclear kinetic energy operator. The process of photodissociation by absorption into the coupled $2^2\Pi$ states is studied theoretically. The adiabatic electronic eigenfunctions and potential energy curves of the $2^2\Pi$ and $3^2\Pi$ states are calculated using large configuration-interaction (CI) representations and the nuclear radial coupling matrix elements are obtained by numerical differentiation. The coupled equations for the nuclear wave functions of the two states are set up in an adiabatic and in a diabatic formulation and are solved by numerical integration. The electric dipole transition moments connecting the ground $x^2\Pi$ state to the $2^2\Pi$ and $3^2\Pi$ states are computed from the CI wave functions and the resulting photodissociation cross sections of OH arising from absorption into the coupled $2^2\Pi$ and $3^2\Pi$ states are obtained. Two alternative sets of potential curves, coupling matrix elements and transition moments are employed to provide an assessment of the accuracy of the results. The photodissociation cross section shows a series of resonances superimposed on a broad continuous background. The resonances are located near to the vibrational levels of the uncoupled bound diabatic potential curve. They have asymmetric Beutler-Fano profiles and vary in width from 50 cm^{-1} for the lowest levels to 2 cm^{-1} for the higher levels. The accuracy of adiabatic and diabatic approximations, carried to first order in the coupling, is

Resonances in the photodissociation of OH by absorption into coupled $2^2\Pi$ states: adiabatic and diabatic formulations

Ewine F. van Dishoeck^a, Marc C. van Hemert^b,

A. C. Allison^{c,d} and A. Delgarno^c.

The coupled equations for the nuclear wave functions of the two states are set up in an adiabatic and in a diabatic formulation and are solved by numerical integration. The electric dipole transition moments connecting the ground $x^2\Pi$ state to the $2^2\Pi$ and $3^2\Pi$ states are computed from the CI wave functions and the resulting photodissociation cross sections of OH arising from absorption into the coupled $2^2\Pi$ and $3^2\Pi$ states are obtained.

Two alternative sets of potential curves, coupling matrix elements and transition moments are employed to provide an assessment of the accuracy of the results. The photodissociation cross section shows a series of resonances superimposed on a broad continuous background. The resonances are located near to the vibrational levels of the uncoupled bound diabatic potential curve. They have asymmetric Beutler-Fano profiles and vary in width from 50 cm^{-1} for the lowest levels to 2 cm^{-1} for the higher levels. The accuracy of adiabatic and diabatic approximations, carried to first order in the coupling, is

^a Sterrewacht Leiden, Huygens Laboratorium, P.O. Box 9513,
2300 RA Leiden, The Netherlands.

^b Department of Physical and Macromolecular Chemistry, Gorlaeus Laboratories, P.O. Box 9502, 2300 RA Leiden, The Netherlands.

^c Harvard-Smithsonian Center for Astrophysics, 60 Garden Street, Cambridge, MA 02138.

^d Department of Computing Science, The University, Glasgow G12 8QQ, Scotland.

explored and it is demonstrated that the diabatic approximation provides a more satisfactory representation of the photodissociation process. The discrete-continuum configuration interaction theory of Fano is applied in the diabatic formulation and the resonance structures are calculated. The discrete-continuum interaction theory yields profile parameters and level shifts which agree well with the accurate values obtained by solving the coupled equations but its application is considerably more laborious. The details of the resonance structures are sensitive to the wings of the adiabatic radial coupling matrix elements, where they depend upon the origin of coordinates. Studies of photodissociation by absorption into strongly coupled electronic states should provide new insight into the nature of the electronic translation factors that are introduced in scattering theory to remove the origin-dependence. The contribution of absorption into the coupled 2^{π} states to the interstellar photodissociation rate is evaluated. In the optically thin limit, the rate is $1.5 \times 10^{-10} \text{ s}^{-1}$. The total rate is $4 \times 10^{-10} \text{ s}^{-1}$.

1. Introduction

Crossings and avoided-crossings of potential energy curves of diatomic molecules are a common occurrence. An example is provided by the potential energy curves of the excited $2^2\Pi$ and $3^2\Pi$ states of the molecule OH, which undergo an avoided-crossing near an internuclear distance of $2.2 a_0'$, a distance which is slightly larger than the equilibrium separation of the ground $X^2\Pi$ state¹. The potential energy curves¹ are illustrated in Fig. 1. Coupling of the two excited states by the radial component of the nuclear kinetic energy operator is expected to be large in the avoided-crossing region.

In the usual picture of photodissociation, absorption into the bound levels of the $3^2\Pi$ state is followed by predissociation into the continuum of the repulsive $2^2\Pi$ state. The coupling of the bound and repulsive states, whether arising from the nuclear kinetic energy operator, or from spin-orbit interactions, is then treated by calculating the predissociation probabilities of the vibrational levels of the bound state using the first-order perturbation Fermi-Wentzel² Golden rule³⁻¹¹. The absorption spectrum consists of a series of discrete lines at the positions of the bound levels which are broadened by predissociation. The validity of this description can be tested by solving the coupled equations for nuclear motion in the excited states.

The coupled equations of nuclear motion for a two-state system with one bound and one continuum state have been solved exactly for a few cases, though mostly for model systems, using either analytical¹² or numerical methods^{13,14}. The bound-continuum systems that have been studied through the coupled equation description include BeH¹⁵, where the excited $B^2\Pi$ state couples with the $2^2\Sigma^+$ and $3^2\Sigma^+$ states through rotational and radial nuclear operators, OH¹⁶ where the $A^2\Sigma^+$ state couples with the $1^4\Pi$, $1^4\Sigma^-$ and $1^4\Sigma^+$ states through spin-orbit interactions and IBr^{14,17} where the $3^3\Pi_{\text{or}}$ states are coupled by the radial nuclear operator. For BeH and OH, line widths and energy shifts were obtained from the variation with energy of the scattering phase shifts across the resonances. For IBr photodissociation cross sections were calculated at a few photon energies. In the IBr calculations, realistic potential energy curves were employed but the adopted coupling matrix element was empirical and the transition dipole moments arbitrary.

We carry out here a detailed study of the dynamics of the coupled $2^2\Pi$ and $3^2\Pi$ states of OH and we obtain accurate predictions of the photodissociation spectrum of OH arising from absorption from the ground state into the coupled $2^2\Pi$ states by solving the equations for nuclear motion in the coupled states using both an adiabatic and a diabatic formulation. We employ potential energy curves, coupling matrix elements and transition dipole moments derived from extensive ab initio calculations. We attempt to obtain an indication of the accuracy of the computed spectra by performing two independent calculations

of the potential energy curves, transition moments and radial couplings. We explore the reliability of the customary perturbation methods by comparing the spectrum resulting from the coupled equations with those obtained from the perturbation theories, and we investigate whether the adiabatic or a diabatic representation provides a better first-order approximation to the process. A preliminary account was given in reference 18.

An additional motivation for studying OH is the importance of accurate photodissociation cross sections of OH in a wide range of atmospheric and astrophysical regimes¹. The photodissociation processes have been studied recently in detail through calculations of the adiabatic potential energy curves of electronic states of $2^2\Sigma^+$, $2^2\Sigma^-$, $2^2\Pi$ and $2^2\Delta$ symmetries, and the electric dipole transition moments connecting them. The repulsive $1^2\Sigma^-$, $1^2\Delta$ and $B^2\Sigma^+$ states were identified as important direct photodissociation channels and the cross sections for absorption from the $X^2\Pi$ state into these states were determined¹. The transition moments to the repulsive $2^2\Pi$ state were found to be very small in the Franck-Condon region of the ground state and of the transitions investigated, the largest oscillator strength was obtained for absorption into vibrational levels of the $3^2\Pi$ state. Previously¹, spontaneous emission into the continuum of the $X^2\Pi$ state was identified as a mechanism for dissociation of the $3^2\Pi$ state vibrational levels, but the

coupling with the repulsive $2^2\Pi$ state through the radial nuclear kinetic energy operator may be more efficient. If so, absorption into the coupled $2^2\Pi$ and $3^2\Pi$ states is an important photodissociation pathway in OH.

II. Theory

We restrict attention to molecular states of the same symmetry coupled by the radial component of the nuclear kinetic energy operator. Then, if we suppress the nuclear angular momentum eigenfunctions, ordinarily specified by the quantum number J , we may write for the total wave function at an energy E measured from the initial state

$$\Psi_E(\underline{r}, R) = \sum_j \psi_j^{\text{ad}}(\underline{r} | R) R^{-1} \chi_j^{\text{ad}}(R) \quad (1a)$$

where \underline{r} represents collectively the position vectors \underline{r}_k of the electrons with the z-axis chosen along the internuclear axis, R is the internuclear distance, $\psi_j^{\text{ad}}(\underline{r} | R)$ is the adiabatic electronic eigenfunction of state j at R , which diagonalizes the fixed-nuclei electronic Hamiltonian, and $R^{-1} \chi_j^{\text{ad}}(R)$ is the corresponding radial nuclear wavefunction. Equation (1a) can be written alternatively in a diabatic form

$$\Psi_E(\underline{r}, R) = \sum_j \psi_j^d(\underline{r} | R) R^{-1} \chi_j^d(R) \quad (1b)$$

For the photodissociation of OH by absorption into the $2^2\Pi$ states at photon energies near 10 eV we need retain only two terms in the expansions. Thus $\psi_1^{\text{ad}} \equiv \psi(2^2\Pi)$ represents the adiabatic $2^2\Pi$ state and $\psi_2^{\text{ad}} \equiv \psi(3^2\Pi)$ represents the adiabatic $3^2\Pi$ state. Similarly, $\psi_1^d \equiv \psi(2^2\Pi)$ represents the diabatic

$2^2\Pi_1$ state and $\psi_2^d \equiv \psi(2^2\Pi_2)$ the diabatic $2^2\Pi_2$ state. For energies less than 14.5 eV, the channel with subscript one is open and the channel with subscript two is closed in both formulations.

We initial ground $X^2\Pi$ state is adequately represented by the wave function

$$\Psi_i(\underline{r}, R) = \psi_i^{\text{ad}}(\underline{r} | R) R^{-1} \chi_i(R) \quad (2)$$

where $\psi_i^{\text{ad}} \equiv \psi(X^2\Pi)$ is the adiabatic electronic eigenfunction of the ground $X^2\Pi$ state and χ_i is the associated discrete vibrational wave function.

The cross section for photodissociation by absorption from the ground state into the $2^2\Pi$ states at a photon energy E is given by

$$\sigma(E) = 2.69 \times 10^{-18} E |\langle \Psi_E | \sum_k z_k | \psi_1 \rangle|^2 \text{ cm}^2 \quad (3)$$

where \square and the matrix element are expressed in atomic units, summation is over all the electrons, and $\langle \dots \rangle$ and $\langle \dots \rangle$ denote integration over respectively the electron and nuclear coordinates. With the adiabatic representation (1a), Eqn. (3) takes the form

$$\sigma^{\text{ad}}(E) = 2.69 \times 10^{-18} E |\langle \Psi_E | \sum_j z_j | \psi_1 \rangle|^2 \text{ cm}^2, \quad (4)$$

where

$$I^d = \langle \chi_1^d \psi(2^2\text{H}) | \sum_k z_k |\psi(x^2\text{n}) \rangle \chi_1 \quad (5)$$

and

$$II^d = \langle \chi_2^d \psi(3^2\text{H}) | \sum_k z_k |\psi(x^2\text{n}) \rangle \chi_2 \quad (6)$$

With the diabatic representation,

$$\sigma^d(E) = 2.69 \times 10^{-18} E |I^d + II^d|^2 \text{ cm}^2 \quad (7)$$

where

$$I^d = \langle \chi_1^d \psi(2^2\text{H}) | \sum_k z_k |\psi(x^2\text{n}) \rangle \chi_1 \quad (8)$$

and

$$II^d = \langle \chi_2^d \psi(3^2\text{H}) | \sum_k z_k |\psi(x^2\text{n}) \rangle \chi_2 \quad (9)$$

The cross section is independent of the representation:
 $\sigma^d(E) \equiv \sigma^{\text{ad}}(E)$.

The adiabatic nuclear wave functions $\chi_j^{\text{ad}}(R)$ satisfy the coupled differential equations expressed in matrix form as 19-21

$$\begin{cases} \frac{d^2}{dR^2} I + K^2 - \frac{J(J+1)}{R^2} I - 2\mu V^{\text{ad}}(R) + B(R) \chi^{\text{ad}}(R) \\ + 2A(R) \frac{d}{dR} \chi^{\text{ad}}(R) = 0, \end{cases} \quad (10)$$

where μ is the reduced mass, I is the unit matrix, $V^{\text{ad}}(R)$ is a diagonal matrix with elements $V_{11}^{\text{ad}}(R)$ and $V_{22}^{\text{ad}}(R)$ which are the adiabatic potential energies, K^2 is a diagonal matrix with elements $K_1^2 = 2\mu [E - V_{11}(^\infty)]$ and $K_2^2 = 2\mu [V_{22}(^\infty) - E]$,

$$A_{jj'} = \langle \psi_j^{\text{ad}} | d/dR | \psi_{j'}^{\text{ad}} \rangle \quad (11)$$

$$B_{jj'} = \langle \psi_j^{\text{ad}} | d^2/dR^2 | \psi_{j'}^{\text{ad}} \rangle \quad (12)$$

the matrix B has non-vanishing diagonal and off-diagonal elements, the antisymmetric matrix A has vanishing diagonal elements. Consistent with expression (4) for $\sigma^{\text{ad}}(E)$, the nuclear wavefunctions satisfy the boundary conditions

$$\chi_1^{\text{ad}}(0) = \chi_2^{\text{ad}}(0) = 0 \quad (13)$$

$$\chi_1^{\text{ad}}(R) \sim \left(\frac{2\mu}{\pi K_1}\right)^{1/2} \sin(k_1 R - \frac{1}{2}\pi + \eta_j) \quad (14)$$

$$\chi_1^{\text{ad}}(R) \sim a \exp(-k_2 R) \quad (15)$$

where ψ_J is the scattering phase shift in the open channel and a is a normalization factor for the closed channel.

The adiabatic and diabatic representations are related by the unitary transformation¹⁹⁻²¹

$$\underline{\psi}^d = \underline{\psi}^ad \underline{C}$$

$$\underline{\chi}(R) = \underline{C}^{-1} \underline{\chi}^ad(R)$$

where \underline{C} is such that the matrix of d/dR in the diabatic basis is the null matrix. Then \underline{C} satisfies the equation

$$\frac{d\underline{C}}{dR} + \underline{A} \underline{C} = 0 \quad . \quad (17)$$

It is convenient to impose the condition that asymptotically $\underline{C} \rightarrow \underline{I}$. In the diabatic representation, the coupled equations for the nuclear wavefunctions take the form

$$\left\{ \frac{d^2}{dR^2} \underline{I} + \underline{K}^2 - \frac{J(J+1)}{R^2} \underline{I} - 2\mu \underline{v}^d(R) + \underline{C}^{-1} \left(\underline{B} - \frac{d\underline{A}}{dR} - \underline{A}^2 \right) \underline{C} \right\} \underline{\chi}^d(R) = 0 \quad , \quad (18)$$

where

$$\underline{v}^d = \underline{C}^{-1} \underline{v}^ad \underline{C} \quad . \quad (19)$$

For a complete basis $\underline{\psi}^ad$,

$$\underline{B} = \underline{A}^2 + \frac{d\underline{A}}{dR} \quad , \quad (20)$$

so the last term in Eqn. (18) vanishes and the diabatic states are coupled only by the off-diagonal elements of the potential matrix $\underline{v}^d(R)$. The diabatic equations are more readily solved numerically than the adiabatic equations.

For the two-state case, the transformation matrix \underline{C} can be written

$$\underline{C} = \begin{pmatrix} \cos \zeta & \sin \zeta \\ -\sin \zeta & \cos \zeta \end{pmatrix} \quad (21)$$

where

$$\zeta(R) = \int_R^\infty A_{12}(R') dR' \quad . \quad (22)$$

The elements of the symmetric matrix $\underline{v}^d(R)$ are expressable as linear combinations of the adiabatic potentials $v_{11}^ad(R)$ and $v_{22}^ad(R)$.

III. Computational methods and results

1. Potential energy curves

The adiabatic electronic wavefunctions $\psi^ad(\underline{x}|R)$ for the OH²₁₁ states were represented by ab initio self-consistent field (SCF) plus configuration-interaction (CI) wavefunctions. Two independent sets of calculations were performed, the details of which can be found elsewhere¹. In short, the first calculation, denoted as the 'Slater calculation', used the ALCHEMY package of programs²² and started from a reasonably large Slater atomic orbital (AO) basis set, which included

polarization and diffuse functions. The molecular orbitals (MO) comprising the CI wavefunctions were those resulting from a SCF calculation for the $1^2\Gamma^-$ state. The final CI wavefunctions contained about 1300 configuration state functions (CSF) and included all single excitations with respect to a set of about ten reference configurations, but only part of the double excitations.

The second set of calculations, denoted as the 'Gaussian calculation', was performed with the Wuppertal-Bonn multi-reference double excitation (MRD-CI) package of programs^{2,3}, and used an AO basis consisting of Gaussian type functions. The CI treatment started with a reference set of configurations from which all single- and double excitation configurations were generated. Those configurations which contributed more, as measured relative to the energy of the reference set, than a predetermined threshold were included directly in the diagonalization procedure, while the remaining ones were taken into account by an extrapolation procedure. The actual computations presented in this paper differ slightly from those reported earlier¹: the MO's were obtained from a SCF calculation for the $1^4\Gamma^-$ state, the reference set of configurations was enlarged to include those with a final CI coefficient greater than 0.07, and the selection threshold was lowered to 15 μ H, ($1H = 1$ Hartree = 27.21ev) resulting in CI matrices of the order of 5000 CSF's.

The potential energy curves for the $X^2\pi$, $2^2\pi$ and $3^2\pi$ states of OH resulting from the Gaussian calculation are presented in Fig. 1. The avoided crossing between the $2^2\pi$ and $3^2\pi$ states around 2.2 \AA_0 is evident. The $2^2\pi$ wavefunction consists mainly of the configuration $(1\sigma)^2 (2\sigma)^2 (3\sigma)^2 (1\pi)^2 [3\Sigma^-] (2\pi)^1$ before the crossing, and of $(1\sigma)^2 (2\sigma)^2 (3\sigma)^1 (4\sigma)^1 [3\Sigma^+] (1\pi)^3$ for larger R values, whereas for the $3^2\pi$ wavefunction the reverse behavior is found. The 2π orbital contains substantial diffuse p character whereas the 4σ orbital is mainly hydrogen anti-bonding. The $X^2\pi$ ground state wavefunction has $(1\sigma)^2 (2\sigma)^2 (3\sigma)^2 (1\pi)^3$ as its principal configuration for distances less than 3.5 \AA_0 . The Slater $2^2\pi$ potential curves show a similar variation with internuclear distance but differ in a few details. As a result of the smaller CI representation¹, the excitation energies for the excited $2^2\pi$ states are about 0.4 ev smaller in the Slater calculation compared with the Gaussian one, the potential well in the $3^2\pi$ state around 2.2 \AA_0 is slightly broader and the position of the minimum in the $3^2\pi$ state is shifted by 0.1 \AA_0 to larger distances.

2. Transition dipole moments

The adiabatic transition moments in Eqns. (5) and (6),

$$D_1^{\text{ad}}(R) = \langle \psi(2^2\Pi) | \sum_k z_k |\psi(X^2\Pi) \rangle \quad (23)$$

$$D_2^{\text{ad}}(R) = \langle \psi(3^2\Pi) | \sum_k z_k |\psi(X^2\Pi) \rangle, \quad (24)$$

obtained in Ref. 1, are illustrated in Fig. 2 for the Gaussian calculation. The sign of the $3^2\Pi - X^2\Pi$ transition moment function, which is arbitrary, is reversed compared with the table in Ref. 1. The transition moments show a strong variation with distance in the region of the avoided crossing.

The diabatic transition moments in Eqns. (8) and (9),

$$D_1^d(R) = \langle \psi(2^2\Pi) | \sum_k z_k |\psi(X^2\Pi) \rangle \quad (25)$$

$$D_2^d(R) = \langle \psi(3^2\Pi) | \sum_k z_k |\psi(X^2\Pi) \rangle, \quad (26)$$

can be obtained from the adiabatic moments by the expressions

$$D_1^d(R) = \cos\zeta(R)D_1^{\text{ad}}(R) - \sin\zeta(R)D_2^{\text{ad}}(R) \quad (27)$$

$$D_2^d(R) = \sin\zeta(R)D_1^{\text{ad}}(R) + \cos\zeta(R)D_2^{\text{ad}}(R) \quad (28)$$

region that occurred for the elements of $D^{\text{ad}}(R)$ is replaced by a smooth behavior of $D^d(R)$.

3. Radial coupling matrix elements

The determination of the radial coupling matrix elements $A_{jj'}(R)$, defined in Eqn. (11), may be accomplished by the evaluation of matrix elements of the one-electron operator $\sum_j z_j/r_j^3$ ²⁴, or by direct numerical differentiation²⁵. The latter method is often more laborious, but it is completely general and for most approximate representations considerably more accurate. We use it here in a slight extension of the procedures outlined in Ref. 25.

We write the CI wave functions for the two states as expressions over CSF's $\phi_K(x|R)$ according to

$$D_j^{\text{ad}}(x|R) = \sum_K c_K^j(R) \phi_K(x|R). \quad (29)$$

The d/dr coupling matrix element can then be computed as the sum of two terms, a CI term and a MO term:

$$\begin{aligned} \langle \psi_1^{\text{ad}} | d/dr | \psi_2^{\text{ad}} \rangle &= \sum_K c_K^1(R) c_K^2(R) \langle \phi_K | \phi_L \rangle \\ &+ c_K^1 c_L^2 \langle \phi_K | d/dr | \phi_L \rangle \\ &= A_{12}^{\text{CI}} + A_{12}^{\text{MO}}, \quad \text{say.} \end{aligned} \quad (30)$$

The diabatic moments corresponding to the Gaussian calculation of $D^{\text{ad}}(R)$ are included in Fig. 2. The rapid variation in the crossing

If the configurations ϕ_K and ϕ_L are constructed from the same set of molecular orbitals, $\langle \phi_K | \phi_L \rangle = \delta_{KL}$ and the CI term simplifies considerably. A finite difference representation may

be obtained by calculating the CI wavefunctions at two slightly different geometries R and $R+\Delta R$ so that

$$\Delta_{12}^{CI}(R) \approx \frac{1}{\Delta R} \left[c_K^1(R) [c_K^2(R+\Delta R) - c_K^2(R)] \right] \quad (31)$$

The MO term can be expanded into matrix elements over molecular orbitals, labelled p for ψ_K and q for ψ_L , the d/dR operator acting as a one-electron operator

where c_{KL} are simple numerical constants which depend on the explicit form of ψ_K and ψ_L . The matrix element $\langle p | d/dR | q \rangle$ is obtained by the same finite difference representation

$$\langle p | d/dR | q \rangle = \frac{1}{\Delta R} [\langle p(R) | q(R+\Delta R) \rangle - \delta_{pq}] \quad (33a)$$

and expansion into the atomic orbital basis functions yields

$$\langle p | d/dR | q \rangle \approx \frac{1}{\Delta R} \left[\sum_U \sum_V d_{up}(R) d_{vq}(R+\Delta R) S_{uv}(R, R+\Delta R) - \delta_{pq} \right] \quad (33b)$$

where d_{up} , d_{vq} are the molecular orbital coefficients and $S_{uv}(R, R+\Delta R)$ is the overlap between the set of atomic orbitals for the molecule at R and $R+\Delta R$.

If the configurations ψ_K and ψ_L were constructed from different SCF wavefunctions, $\langle \psi_K | \psi_L \rangle = S_{KL}$ and the CI term according to Eqns. (30) - (33)²⁵.

retains the double summation. The dc_L^2/dR term can again be obtained with finite differences. In the MO term, the matrix element R_{pq}^{KL} is replaced by x_{pq}^{KL} which not only contains the permutational coefficients, but also the cofactors of the MO overlap matrix at R formed by the MO's. Since $\langle p(R) | q(R) \rangle \neq \delta_{pq}$ in this case, the second term in Eqns. (33) is also much more complicated.

Although the splitting into the non-physical CI and MO contributions is computationally convenient if a common set of MO's is used, it can be avoided. Direct application of finite differences to the electronic wavefunctions, based either on the same or on different sets of orbitals, gives

$$\langle \psi_1^{ad} | d/dR | \psi_2^{ad} \rangle \approx \frac{1}{\Delta R} [\langle \psi_1^{ad}(R) | \psi_2^{ad}(R+\Delta R) \rangle - \langle \psi_1^{ad}(R) | \psi_2^{ad}(R) \rangle] \quad (34)$$

For large CI wavefunctions the second term should be small and may be negligible. The first term is expanded as

$$\begin{aligned} \langle \psi_1^{ad}(R) | \psi_2^{ad}(R+\Delta R) \rangle &= \sum_K \sum_L c_K^1(R) c_L^2(R+\Delta R) \langle p(R) | q(R+\Delta R) \rangle \\ &= \sum_K \sum_L c_K^1(R) c_L^2(R+\Delta R) \sum_P \sum_Q x_{pq}^{KL}(R, R+\Delta R) \langle p(R) | q(R+\Delta R) \rangle \end{aligned} \quad (35)$$

where now the MO overlap matrix at $(R, R+\Delta R)$ has to be evaluated for the construction of the cofactors in x_{pq}^{KL} .

In the Gaussian calculation, the matrix element $\langle \psi(2^2\Pi) | d/dR | \psi(3^2\Pi) \rangle$ was obtained as the sum of the CI and MO terms according to Eqns. (30) - (33)²⁵. The magnitude of the radial

coupling matrix element depends on the choice of the origin with respect to which the electronic coordinates are kept fixed when the derivative is taken^{21,24}. The matrix elements for different origins are related by the product of the energy difference of the two states and the electronic transition dipole matrix element $\langle \psi(2^2\pi) | \hat{z}_j | \psi(3^2\pi) \rangle$ ²¹. In our application, the choice of origin must be made with reference to the coupled equations (10) and (18), which were formulated with the center of mass as the origin. In the Gaussian calculations of $A_{12}(R)$, the term relating the matrix elements for different origins is very small and we took the oxygen nucleus as the origin. The insensitivity to the choice of the origin occurs because only the MO-term in Eqn.(30) is origin-dependent, and in the present case the CI-term contributes more than 90% to the total A_{12} .

The result of the Gaussian calculation for A_{12} is presented in Fig. 3 as a function of internuclear distance in the region of the avoided crossing. In obtaining the electronic eigenfunctions, the threshold was set at 30 μH , which reduced the CI expansion to about 3000 terms, and an interval $\Delta R = 5 \times 10^{-5} a_0$ was used. The coupling was also obtained with a smaller CI expansion of about 2000 CSF's, corresponding to a selection threshold of 50 μH . It is slightly smaller at the peak and shifted to shorter distances by about $0.01 a_0$. Both curves show the characteristic Lorentzian profile expected for a simple two-

state approximation when the CI term dominates the coupling matrix element²⁶. They have a FWHM of about $0.045 a_0$.

In the Slater calculation, the coupling matrix element was determined with a modified version of the ALCHEMY transition moment package. The modifications consisted mainly of the replacement of the AO dipole moment operator matrix at the appropriate places by the AO overlap matrix, either at R, or in the double basis set, at R and R+ΔR. Since the ALCHEMY package has the capability of calculating the transition moments based either on one common set of MO's or on different sets of MO's for the two states, the same versatility was easily realized for the computation of the d/dR matrix element. Moreover, it enabled us to construct a program in which the matrix element is calculated directly, without the splitting into the CI and MO terms contained in Eqn. (30), thus avoiding problems in the determination of the sign of each of the separate terms.

The results of the Slater calculation for the coupling matrix element are included in Fig. 3. The same CI wavefunctions as those employed in the potential curves were used, the center of mass was chosen as the origin, and $\Delta R = 2 \times 10^{-4} a_0$ was taken. The sensitivity to the choice of MO's, especially the possibility of taking different MO's for the two states, was not further explored. The Slater coupling function shows a similar Lorentzian profile to the Gaussian coupling function, apart from a shift to larger distances, consistent with the shift in the minima of the corresponding potential curves. It has a

slightly larger FWHM of about $0.05 a_0$. If the two-state model of an avoided crossing is indeed applicable, the integral of the radial coupling over R equals $\pm \pi/2$, as long as the MO-term contribution to the coupling is negligible.²⁶ The integral of the Slater radial coupling between 2.1 and 2.4 a_0 is $-0.94 \pi/2$ and the integral of the Gaussian coupling between 2.0 and $2.35 a_0$ is $-0.82 \pi/2$. Both values are close enough to $-\pi/2$ that the remaining differences can be attributed to the wings of the functions outside the ranges of integration for which calculations were made. The closeness to $-\pi/2$ and the agreement between the two independent calculations suggest that the computed matrix-elements are accurate. In the next sections we will investigate whether the level of accuracy achieved for the couplings is adequate for determining the details of the photodissociation cross sections.

4. Nuclear wavefunctions

The two second-order adiabatic coupled equations (10) for the nuclear wavefunctions χ^{ad} were transformed to four first-order coupled differential equations and integrated numerically using the fourth-order Runge-Kutta method. Because the solution $\chi_2^{\text{ad}}(R)$ is a decaying exponential, integration in the direction of increasing R is unstable. Thus forward integration from $R = R_0$ and backward integration from $R = R_f$, a distance where the decaying exponential is sufficiently small, with a matching at

some intermediate point were employed. An obvious choice for the matching point is the distance where the avoided crossing of the states occurs. The integration of the open channel equation for $\chi_1^{\text{ad}}(R)$ was then continued from R_f for increasing R until the phase shift had converged. Because the equations are linear, unnormalized solutions were obtained, which were normalized to the required form of the oscillatory function $\chi_1^{\text{ad}}(R)$ at the end of the calculation.

The diabatic coupled equations (18) for the nuclear wavefunctions χ^{d} were integrated numerically using the Numerov method. The solution of the diabatic equations proceeded otherwise along the same lines²⁵ as for the adiabatic equations. The integration step size used for the adiabatic equations, $0.0025 a_0$, was one half that for the diabatic equations, $0.005 a_0$, for comparable accuracy. A check on the programs is provided by a comparison of the phase shifts of the open channels in the two formulations, which should be identical.

For the potentials V^{ad} and the coupling term A , which enter the adiabatic equations and the transformation to the diabatic equations, we used the computed values described in the preceding sections. Because the ab initio calculation of the second-derivative matrix B is very cumbersome²⁵, it was replaced by $A^2 + dA/dR$. With this choice, the last term in the diabatic equations (18) vanishes, and the radial coupling element A_{12} is utilized only in the transformation from the adiabatic to the diabatic representation. The identity of the matrices B and $A^2 + dA/dR$ holds only for a complete set χ^{ad} . Provided the coupling

to the other π states is small, as we assume, the use of the identity should be an adequate approximation even with our limited set.

The nuclear wavefunctions resulting from the adiabatic and diabatic coupled equations at an energy of 4.0 ev above the dissociation limit of the $2^2\pi_{11}$ state, obtained with the potential curves and radial coupling function from the Slater calculation, are illustrated in Fig. 4. In the calculations, J was taken equal to zero.

5. Photodissociation cross sections

After having solved the coupled equations for the nuclear wavefunctions of the excited $2^2\pi$ states, either in the adiabatic or diabatic formulation, the cross sections for absorption from the ground $x^2\pi$ state into the coupled excited states can be calculated using Eqns. (4)-(9). Care must be taken of the relative signs of the transition moments and radial coupling matrix elements, since cross terms appear in the equations for σ^{ad} and σ^{d} . The signs of the adiabatic $2^2\pi_1-x^2\pi_1$ and $3^2\pi_1-x^2\pi_1$ transition moments shown in Fig. 2 were adopted. The sign of the $2^2\pi_1-3^2\pi_1$ radial coupling element is then no longer arbitrary, but must be negative, as indicated in Fig. 3. The corresponding transformation parameter ζ varies from about $-\pi/2$ to 0 through the crossing region. The resulting diabatic $2^2\pi_1-x^2\pi_1$ and $2^2\pi_1-x^2\pi_1$ transition moments are indicated in Fig. 2.

In the computations, the transformation parameter $\zeta(R)$ was forced to be within 18 of $-\pi/2$ for R values less than $R_e = 1.85 a_0$. Thus the diagonal diabatic couplings V_{12}^d , together with those obtained with the Slater ab

potentials coincide with the adiabatic potentials in the Franck-Condon region of the ground state. With the Slater radial coupling this was effected by choosing appropriate extrapolations of the calculated coupling for small and large R -values. For the radial coupling function obtained with the Gaussian calculation the same procedure may be followed, but a simpler method is to approximate the ab initio values by a Lorentzian formula

$$A_{12}(R) = \frac{-W/4}{(R-R_C)^2 + \frac{1}{4}W^2}, \quad (36a)$$

with width W and integral $-\pi/2$, centered at $R=R_C$. The Lorentzian lineshape with $W = 0.05 a_0$ is included in Fig. 3. In order to investigate the sensitivity of the results to the short and long range behavior of the couplings, we have also studied the extreme case of a Gaussian lineshape

$$A_{12}(R) = -\frac{(\pi b)^{1/2}}{2} \exp \left\{ -b(R-R_C)^2 \right\} \quad (36b)$$

with width $b^{-1/2}$ and integral $-\pi/2$, even though it appears not to be realistic in view of the ab initio results and theoretical considerations²⁶. The Gaussian coupling for $b \approx 500 a_0^{-2}$ is illustrated in Fig. 3. For both the Lorentzian and the Gaussian formula, the transformation parameter ζ can be expressed analytically in terms of an arc cotangent and a complementary error function, respectively. The corresponding diabatic couplings V_{12}^d , together with those obtained with the Slater ab

initial radial coupling, are illustrated in Fig. 5. The potential couplings between the diabatic states obtained with the Slater radial coupling or with the Lorentzian formula extend over a much larger distance than the nuclear radial couplings between the adiabatic states, and do not show a pronounced peak at $R=R_C$. Only the Gaussian formula for the radial coupling results in a diabatic coupling which is confined to a narrow region around the crossing.

The photodissociation cross sections for absorption from the $v''=0$ vibrational level of the χ_{11}^2 state into the coupled excited χ_{11}^2 states are presented as functions of incident photon energy in Fig. 6a and b for the Slater and Gaussian calculations, respectively. The cross sections shown were obtained with the diabatic formulation. Identical cross sections result from the adiabatic formulation, as they must. In both figures, the cross section shows a regular background superimposed on which is a series of resonances. The background cross sections in the two calculations agree well apart from the expected shift of about 0.4 eV due to the different excitation energies. They were found to be very insensitive to the precise shape, whether Lorentzian or Gaussian, of the radial coupling function, as long as the integral was close to $-\pi/2$ in the Franck-Condon region of the ground state. In the diabatic formulation, the term r^d in σ^d , corresponding to absorption into the diabatic continuum, is much larger than r^d , except at the lowest few resonances. In the adiabatic formulation, the opposite behavior is found, as could be anticipated from inspection of the wave functions of Fig. 4 around R_e .

The resonances occur with a spacing ranging from about 3000 cm⁻¹ for the first resonances to 800-1000 cm⁻¹ for the higher ones. They have asymmetric Beutler-Fano lineshapes, arising from the interference between a bound and a continuum state when both carry an oscillator strength^{3,27}. All resonances have a minimum close to zero, and most have a maximum larger than 10^{-17} cm².

The positions of the resonances may be compared with the positions of the vibrational levels of the uncoupled bound adiabatic $3^2\Pi$ and diabatic $2^2\Pi_2$ potential curves. Fig. 7 shows an enlargement of the adiabatic Gaussian potential curves in the region of the avoided crossing with the positions of the lowest 12 vibrational levels indicated. The dashed lines show the diabatic diagonal potentials and the corresponding diabatic vibrational levels. There are two diabatic vibrational levels lying below the first adiabatic level. For higher vibrational quantum numbers the adiabatic and diabatic levels come into coincidence. The full arrows in Fig. 6a and b are located at the energies of the uncoupled diabatic vibrational levels. They agree closely with the positions of the resonances. The dashed arrows indicate the energies of the first two adiabatic vibrational levels. They do not coincide with any of the resonances.

The locations of the diabatic energy levels and of the associated resonances, and the shape of the absorption spectrum, though insensitive to the shape of the adiabatic radial coupling function $A_{12}(R)$ are sensitive to the magnitude of its integral over R .

If the integral of A_{12} is not $\pm\pi/2$, as we have required, the diabatic curves will not merge with the adiabatic curves at separations inside the crossing region, which are the most important for determining the shape of the spectrum, and the diabatic energy levels will be shifted. Because the Franck-Condon region lies inside the crossing region the spectrum shape may differ substantially. An additional uncertainty in A_{12} arises because it depends upon the origin of the nuclear coordinates. Although the dependence was found to be small near the peak values of the radial coupling, it has considerable influence on the wings of the coupling, and may change the integral by several percent. The introduction of electronic translation factors²⁸ in the specification of the electronic eigenfunctions removes the origin-dependence, but substantially complicates the calculation. It will be of interest to study the effects of different translation factors on the calculated absorption spectrum.

IV. Approximate methods

1. The matrix B

In the adiabatic formulation, the matrix B is often neglected. Fig. 8 shows the photodissociation cross section for the Gaussian calculation that is obtained if the matrix B , or $A^2 + dA/dR$, is equated to zero. The resulting spectrum is markedly different from the exact one shown in Fig. 6b, emphasizing the importance of retaining B if the coupled equations are solved in the adiabatic formulation. If B is neglected, the adiabatic and diabatic equations are only compatible when the term $C^{-1}(-A^2 dA/dR)C$ is retained in the diabatic formulation.

2. Adiabatic approximate methods

The approximate method most often used in the study of adiabatic nuclear interactions between a bound and a repulsive state is first-order perturbation theory starting from the adiabatic representation. In this approximation, absorption takes place into discrete vibrational levels v' of the adiabatic bound 3Π state, which subsequently undergo predissociation to the repulsive $2^2\Pi$ state with a rate k_v^{ad} , given by the Fermi-Wentzel Golden rule²

$$k_v^{\text{ad}} = 4.13 \times 10^{16} \frac{2\pi}{\hbar} |(\chi_1^0(E_{v'}))| A_{12} d/dR |\chi_2^0(E_{v'})| + \frac{1}{2} (\chi_1^0(E_{v'})) |B_{12}| \chi_2^0(E_{v'})|^2 s^{-1} \quad (37)$$

where the nuclear wavefunctions $\chi_j^0(E_{v'})$ are the solutions of the uncoupled radial eigenvalue equations containing the adiabatic $2^2\Pi$ and $3^2\Pi$ potentials respectively, evaluated at the energy $E_{v'}$ of the v' bound vibrational level, and all quantities are in atomic units. The term containing the second derivative coupling B_{12} in (37) is often neglected but its effects can be large. The line width Γ_v^{ad} is related to the predissociation rate by

$$\Gamma_v^{\text{ad}} = 5.3 \times 10^{-12} k_v^{\text{ad}} \text{ cm}^{-1} \quad (38)$$

Table I lists the calculated predissociation rates and widths for v' ranging from 0 to 16 using either the Slater potential curves and the Slater ab initio radial coupling or the Gaussian potential curves and the Gaussian ab initio radial coupling, approximated by the Lorentzian formula with $w = 0.05 a_0$. As in the coupled equations, the B_{12} coupling was approximated by dA_{12}/dR . The rates and line widths show a general decrease with a weakly oscillatory

behavior with v' , and differences by orders of magnitude occur in the rates for the various vibrational levels. The rates for particular levels v' obtained with the two ab initio calculations also show large differences. Previous studies 4-7 have demonstrated the sensitivity of individual rates to the position and shape of the potential curves and coupling function, even when the potential curves do not cross and may lie far apart^{6,9}.

The predissociation rates are all larger than 10^{11} s^{-1} , and are mostly of the order of 10^{13} s^{-1} . They are much larger than the rates for spontaneous emission¹ into the ground $X^2\Pi$ state vibrational levels of 10^8 - 10^9 s^{-1} so that, despite the uncertainties in the individual predissociation rates, it is clear that predissociation occurs with unit efficiency. However, the high rates of predissociation indicate that the coupling is so strong that a first-order perturbation treatment starting from the adiabatic uncoupled representation may not be valid.

Also indicated in Table I is the predissociation rate obtained by taking only the $A_{12} d/dR$ term in Eqn. (37) into account. The rate varies more irregularly with v' and the B_{12} term may increase or decrease the total rate by as much as an order of magnitude.

With the calculated line widths Γ_v^{ad} , the absorption or photodissociation spectrum can be constructed by assuming a Lorentzian lineshape for absorption from the $v'' = 0$ vibrational level of the $X^2\Pi$ state into each of the vibrational levels v' of the $3^2\Pi$ state

$$\sigma_0^{\text{ad}}(E) = 4.03 \times 10^{18} \frac{r_v^{\text{ad}}}{v'} \frac{2\pi r_v^{\text{ad}}}{(E-E_{v'})^2 + r_v^{\text{ad}}/4} \text{ cm}^2, \quad (39)$$

where r_v^{ad} and $E_{v'}$ are in hartrees. The absorption oscillator strengths $f_{0v'}^{\text{ad}}$ for the two calculations are included in Table I. The resultant spectrum for the Gaussian calculation is presented in Fig. 9. The differences from the exact spectrum of Fig. 6b are considerable, indicating that the conventional treatment of adiabatic radial interactions in predissociation is inadequate here. The direct photodissociation cross section for the $2^2\Pi$ state¹ is included in Fig. 9. Because of the small transition moment in the Franck-Condon region, the direct absorption is insignificant.

3. Diabatic approximate methods

Once the adiabatic potential energy curves and radial coupling function have been computed, the transformation to a diabatic basis is easily accomplished. Since the diabatic $2^2\Pi_1$ potential is repulsive everywhere, and the $2^2\Pi_1 - X^2\Pi$ diabatic transition moment, shown in Fig. 2, is large in the Franck-Condon region, we may envisage direct photodissociation by absorption into the uncoupled diabatic state. The resultant cross sections of the two calculations starting from the $X^2\Pi(v''=0)$ level are presented in Fig. 10. They are identical to the background cross sections of Figs. 6a and 6b. Table II lists the cross sections for the Gaussian calculation.

First order perturbation theory may also be utilized for the calculation of the predissociation rates for the vibrational levels of the bound diabatic $2^2\Pi_2$ curve. The adiabatic couplings in Eqn. (37) have to be replaced by the off-diagonal diabatic V_{12}^d potential and the adiabatic uncoupled nuclear wave functions followed and an absorption spectrum can be constructed. The diabatic absorption oscillator strengths $f_{0v'}^d$, predissociation probabilities $k_{v'}^d$, and widths $\Gamma_{v'}^d$ for the diabatic $2^2\Pi_2$ state can be derived from tables III and IV. The predissociation rates are about 10^{13} s^{-1} for the low-lying levels decreasing to 10^{12} s^{-1} for the higher levels and absorption into the diabatic bound vibrational levels leads to dissociation with unit probability.

The sum of the cross sections for the uncoupled $2^2\Pi_1$ state and the predissociated $2^2\Pi_2$ state is shown in Fig. 11 for the ab initio Gaussian calculation. Because the oscillator strengths for the diabatic bound vibrational levels are very small for $v' > 0$, as are the line widths, the contributions of these levels appear as small, sharp peaks on top of the continuous cross section at the positions of the diabatic vibrational levels. Although the positions of the peaks are close to the actual resonances, their shape does not agree. Nevertheless, it is evident that the diabatic representation gives a much better first order approximation than does the adiabatic representation.

V. The Resonances

All the resonances in Fig. 6a and 6b have the asymmetric Beutler-Fano lineshape, resulting from the interference of the bound and continuum wavefunctions. The individual resonance structures are very different, as Fig. 12 demonstrates, and they may depend in detail on the particular calculation. The first resonance in both calculations, corresponding to $v'=0$ of the bound diabatic state, has a very large broad maximum, whereas the second resonance, corresponding to $v'=1$, has a very broad minimum with a small maximum.

In the Slater calculation of Fig. 6a, the third and fourth resonances, corresponding to $v'=2$ and 3, rise first to a maximum and then fall rapidly to zero, whereas for the remaining resonances $v' \geq 4$ the reverse behavior is found. We denote the behavior for $v'=2$ and 3 by a "+/- profile", that for $v' \geq 4$ by a "-/+ profile." In the Gaussian calculation of Fig. 6b, the resonances up to $v'=6$ have a "+/" profile, while the "-/+" profile occurs for $v' \geq 7$. Thus, the shapes of the resonances are sensitive to the potential curves and couplings.

In order to study these effects in more detail, we have explored several possible combinations of curves and couplings. The resonances up to $v'=16$ were investigated. The main influence on the behavior of the resonances is exerted apparently by the couplings, not by the potential curves: if the Slater ab initio coupling matrix element, shifted to correct for the difference in position of the crossing in the two calculations, is adopted together with the Gaussian potential curves, the same "+/" behavior is found as with the Slater curves. If a

Gaussian lineshape with $b = 500 \text{ a}_0^{-2}$ is adopted for the coupling together with the Gaussian potential curves, a different behavior is found, with reversals in the shape of the resonances occurring after $v'=2$, 9 and 15. If the parameter b in the Gaussian formula for the coupling is lowered from $b \approx 500 \text{ a}_0^{-2}$ to $b \approx 30 \text{ a}_0^{-2}$, corresponding to a substantial broadening of the coupling, the first reversal shifts to larger v' values and the others disappear. Clearly, the long and short range wings of the coupling play an important role in determining the behavior of the resonances.

To gain more insight into the mechanism which is triggering the reversals, the resonance profiles were analyzed using a configuration-interaction description of the interference between bound and continuous absorption given by Fano²⁷. According to it, the resonance profile may be expressed in the form

$$\gamma_{v'}(\epsilon) = \frac{(q_{v'} + \epsilon)^2}{(1 + \epsilon^2)} \quad (40)$$

where ϵ is a reduced energy variable,

$$\epsilon = \frac{E - E_{v'} - F(E_{v'})}{\Gamma_{v'}/2} \quad (41)$$

$F(E_{v'})$ is an energy shift and $q_{v'}$ is a shape parameter which characterizes the profile for each vibrational level v' of the bound state.

In the theory, the width $\Gamma_{v'}$ is obtained according to

$$\Gamma_{v'} = 2\pi |V(E_{v'})|^2 \quad (42)$$

where $V(E_{v'})$ is the interaction matrix element between the uncoupled bound and continuum states at an energy $E = E_{v'}$.

In the diabatic representation,

$$V(E_{v'}) = (\chi_1^0(E_{v'})) |V_{12}| \chi_2^0(E_{v'}) \quad (43)$$

where $\chi_j^0(E_{v'})$ are now the solutions of the uncoupled equations containing the repulsive $2\pi l_1$ and bound $2\pi l_2$ diagonal potentials respectively determined at $E = E_{v'}$. The energy shift is given by the principal value integral

$$F(E_{v'}) = P \int_0^\infty \frac{|V(E')|^2}{E_{v'} - E'} dE' \quad (44)$$

where

$$V(E') = (\chi_1^0(E')) |V_{12}| \chi_2^0(E_{v'}) \quad (45)$$

The shape parameter for each resonance depends upon the ratio of the vibrationally averaged transition moments D_2^d and D_1^d respectively to the bound vibrational level v' and the continuum at $E = E_{v'}$,

$$D_j^d(E_{v'}) = (\chi_j^0(E_{v'})) |D_j^d| \chi_1^0 \quad (46)$$

according to

$$q_{v'} = \frac{\bar{D}_2^d(E_{v'}) + G(E_{v'})}{\pi V(E_{v'}) \bar{D}_1^d(E_{v'})} \quad (47)$$

The second term in the numerator,

$$G(E_{v'}) = P \int_0^\infty \frac{V(E') \bar{D}_1^d(E')}{E_{v'} - E'} dE' \quad , \quad (48)$$

involves the admixture of continuum wavefunctions to the uncoupled bound state wavefunction weighted by the discrete-continuum-interaction.

All the terms in q and ϵ can be evaluated numerically from the potential curves, transition moments and interaction matrix elements. Because the relative signs of the individual terms are significant, care must be taken to ensure consistency. The integrals $P(E_{v'})$ and $G(E_{v'})$ were obtained by excluding a region of dimension δ around $E_{v'}$, evaluating numerically the integrals for several values of δ and extrapolating to $\delta = 0$. The values of $q_{v'}$, and of each of the two terms in its numerator, $\bar{D}_2^d(E_{v'})$ and $G(E_{v'})$, corresponding to the Slater potentials and couplings, to the Gaussian potentials with the Lorentzian formula (36a) for the coupling and to the Gaussian potentials with the Gaussian formula (36b) for the coupling, are collected in Table III. The factors $V(E_{v'})$ and $\bar{D}_1^d(E_{v'})$ entering into the denominator of $q_{v'}$ are listed in Table IV.

Each of the terms of q_1^d , except D_1^d , changes sign often for different vibrational levels v' and the behavior depends upon the potential curves and coupling elements. However, the variation of $q_{v'}$ with v' is more regular and $q_{v'}$ represents correctly the behavior of the resonances except in one instance close to a change in sign of $q_{v'}$. The sign of $q_{v'}$ is sufficient to establish the $+/-$ or $-/+$ behavior of the profile. If $q_{v'}$ is negative, the $-/+$ profile occurs, if $q_{v'}$ is positive the $-/+$ profile.

In all cases, the first sign change in $q_{v'}$ for $v' > 1$ coincides with a sign change in $V(E_{v'})$. For the ab initio Slater and the Lorentzian radial couplings, which correspond to very broad diabatic couplings (cf. Fig. 5), no other reversal is found up to $v'=16$, even though $V(E_{v'})$ does change sign. For higher v' , the numerator is dominated by $G(E_{v'})$, which contains $V(E')$ in the integrand and which changes sign at the same v' as $V(E_{v'})$ does, resulting in no net change in the sign of $q_{v'}$. For the Gaussian formula for the coupling, which corresponds to the narrow diabatic coupling and consequently to smaller values of $V(E_{v'})$, the situation is more complicated and no term in $q_{v'}$ dominates the behavior.

Although the configuration-interaction theory correctly predicts the profile characteristics, it appears that we gain little from an inspection of the individual terms. Any one of them may dominate at a particular value of v' .

For the Fano profile, the cross section is zero at $\epsilon = -q$ and has its maximum value $q^2 + 1$ at $\epsilon = 1/q$. Table V lists the q values, derived from the height of the maximum of the resonance in the coupled equations relative to that of the uncoupled continuum cross section, with those obtained from the Fano theory. The agreement is very good, generally within a few percent, except for a few levels close to a reversal in the lineshape, where $V(E_{v'})$ varies rapidly. Both the Fano theory and the coupled equations show a large range in q values for the various vibrational levels, especially for the lower ones where the interference effects are largest.

In table VI, the calculated energy shifts $F(E_{v'})$ are compared with the shifts found from solving the coupled equations. For the coupled equation solutions the resonance position was taken to be the energy where the phase shift η for χ_1^d differed by $\pi/2$ from the phase shift η^o of the uncoupled continuum diabatic wavefunction $\chi_1^o(E')$. Subtraction of the energy $E_{v'}$ of the uncoupled diabatic bound vibrational level then yields the shift. The agreement establishes the validity of the Fano theory for the description of the

resonances. The energy shift for the $v'=0$ vibrational level, which lies below the crossing point of the diabatic curves, is negative in all cases, as was found in other studies^{7,8,17,29}. The shifts obtained with the Gaussian formula for the coupling are an order of magnitude smaller than those for the other couplings.

Fig. 12 illustrates the profiles resulting from the coupled equations together with those obtained with the Fano theory for $v'=0-4$ and one of the higher resonances, $v'=10$, for the Slater calculation with the ab initio radial coupling. The broad high maximum of the $v'=0$ resonance occurs in the Fano theory because the numerator of q , in particular the transition moment to the diabatic bound state, and $V(E_{v'})$ are large. The large $q_{v'}$ values which are found for some of the higher v' levels result not from a large transition moment in the numerator, but from a small interaction term $V(E_{v'})$ in the denominator. The corresponding profiles are high and narrow and do not resemble the $v'=0$ resonance. For the $v'=1$ resonance, the numerator of q is about an order of magnitude smaller than for $v'=0$, leading to a very small value of q . The linewidth¹ is large and the resonance broad.

All the resonance profiles in the coupled equations appear to be fitted satisfactorily by the Fano lineshape and the assumption that $q_{v'}$ and $F(E_{v'})$ can be regarded as constant with energy in the range of the resonance is valid. If they had varied considerably over the resonance, a distorted

Fano profile would have resulted²⁹, which is not found for any of the resonances. We checked that indeed the matrix elements changed by less than 1% across a resonance, except in one case where the resonance happened to coincide with a change of sign of the matrix element $V(E_{v'})$.

Although the discrete-continuum interaction theory apparently gives very good quantitative results, the calculation of the $F(E_{v'})$ and $G(E_{v'})$ integrals is a laborious procedure, since for every v' the integration over the whole energy range has to be performed. From the experimental point of view, the resonance structures can be conveniently analyzed in terms of widths and shape parameters, but theoretically it is simpler and more general to solve the coupled equations of the excited states to describe the resonances than to use the method of Fano, as was noted previously^{14,15} for the calculation of $F(E_{v'})$. The necessary computer time is comparable for the two methods, and is several orders of magnitude less than that for the ab initio calculations of the potential energy curves, transition moments, and radial coupling function.

VI. The interstellar photodissociation rate

Photodissociation by absorption into the coupled 2^2_{\parallel} and 3^2_{\parallel} states contributes importantly to the interstellar photodissociation rate. With the unattenuated radiation field adopted previously^{30,1}, the cross sections listed in Table II yield a rate of $1.5 \times 10^{-10} \text{ s}^{-1}$. This value replaces the rates of $1.2 \times 10^{-10} \text{ s}^{-1}$ and $0.09 \times 10^{-10} \text{ s}^{-1}$ given in

Table XIV of Ref. 1 for the adiabatic $3^2\Pi$ and $2^2\Pi$ states. The total rate is about $4 \times 10^{-10} \text{ s}^{-1}$. Because the cross section is continuous, self-shielding is negligible in the $2^2\Pi$ channel.

VII. Concluding Remarks

In cases of strong coupling between adiabatic molecular states, a diabatic zero-order representation of the dissociation provides a more realistic description of the dissociation process. If one of the diabatic states contains bound energy levels, absorption can be regarded as a direct process into the continuum of the repulsive diabatic state modified by temporary captures into the discrete levels of the attractive diabatic state which decay by predissociation. The resonances are located at specific energies and have specific widths and shapes. When absorption is stronger than the repulsive state, the spectrum consists of a smooth background with a superposition of diabatic vibrational resonance structures. When absorption occurs to both diabatic states, the resonances have asymmetric profiles.

The absorption spectra of Figs. 6a and 6b, obtained using respectively the Slater and Gaussian calculations, are in general agreement, except for some minor aspects of the resonances. The locations, shapes and widths of the resonance profiles appear to depend on the values of the adiabatic

radial coupling matrix elements. Tables V and VI show the differences in shifts and line shape parameters for the two calculations. The results are particularly sensitive to the wings of the coupling function outside the crossing region, which are not only hard to obtain accurately in the ab initio calculations, but which also depend on the choice of origin of the coordinates.

In our calculations, we have neglected couplings to other states. The $3^2\Pi$ state undergoes avoided crossings with higher-lying $2^2\Pi$ states at separations of about 2.0 a_0 and 3.0 a_0 and with the ground $X^2\Pi$ state near 3.5 a_0 . A diabatic description is appropriate for the first two avoided crossing regions and an adiabatic description for the third. With the inclusion of these couplings, the diabatic $2^2\Pi_1$ repulsive curve will be little changed, but the diabatic $2^2\Pi_2$ bound curve will not flatten at 3 a_0 . The vibrational levels of the $2^2\Pi_2$ curve will be shifted and will have larger spacings. There also exist at similar excitation energies $2\Sigma^-$ states and the $B^2\Sigma^+$ state which can be coupled by rotational motion. High resolution will be needed to separate out the several interactions.

The interaction between the $3^2\Pi$ and the higher $2^2\Pi$ states at 3 a_0 will also give rise to a diabatic curve which has its minimum at a large internuclear distance around 3.5 a_0 . The lower vibrational levels of this diabatic state are not expected to interact strongly with the repulsive $2^2\Pi_1$ state and may decay by spontaneous emission into the higher vibrational

levels of the $X^2\Pi$ state with rates which are close to those calculated for the adiabatic $3^2\Pi$ vibrational levels¹. The transitions may explain some of the strong unidentified lines that have been seen near 185 nm.³¹

We have not explored the modifications caused by the distribution of rotational levels in the initial state, but at low resolution the superposition of the resonances arising from absorption out of individual rotational levels will cause an apparent broadening of the resonance profiles and may suppress the interference effects. Asymmetric Fano profiles have been identified so far only in the absorption of molecular hydrogen into the $B^1\Sigma_u^+$ and $D^1\Pi_u$ states arising from interactions with the $B^1\Sigma_u^+$ state.³²⁻³⁶

The resonance phenomenon arising from interacting molecular states is a general one. Examples of molecules where adiabatic molecular states interact by the nuclear kinetic energy operator are BeH₅ ($B^2\Pi$, $2^2\Sigma^+$ and $3^2\Sigma^+$ states), C₂¹⁷ ($3(F)1\Pi_u$ and $2^2\Pi_u$ states), O₂^{25,38} ($1(B)3\Sigma_u^-$ and $2^3\Sigma_u^-$ states), N₂⁹ ($B^2\Sigma_u^+$ and $C^2\Sigma_u^+$ states), Li⁺₂³⁹ ($2^2\Sigma_u^+$ and $2^1\Pi_u$ states) and IBr and IC₁ ($3\Pi_{g+}$ states)⁴⁰.

Acknowledgments

The authors are indebted to Professors R. J. Beunker and S. D. Peyerimhoff for the use of their sets of programs. This work was supported by the Netherlands Organization for the Advancement of Pure Research (ZWO) and by the National

Table I. Absorption oscillator strengths f_{0v}^{ad} , predissociation probabilities k_v^{ad} , in s^{-1} and linewidths r_v^{ad} , in cm^{-1} as functions of vibrational level v' of the adiabatic $3^2\Pi$ state for two different calculations.

$v' 10^3 f_{0v}^{\text{ad}}$	Slater ^a			Gaussian ^b			Photon energy (eV)	$\sigma^d (10^{-18} \text{ cm}^2)$
	r_v^{ad}	$10^3 k_v^{\text{ad}}$	$10^3 r_v^{\text{ad}}$	r_v^{ad}	$10^3 k_v^{\text{ad}}$	$10^3 r_v^{\text{ad}}$		
0	1.27	582.5	11.00	41.70	2.01	1367.8	25.80	37.90
1	2.47	3227.2	60.80	8.77	4.24	2667.6	50.20	5.93
2	2.71	1005.0	19.00	46.40	0.86	3427.7	6.45	4.16
3	2.06	389.6	7.34	29.70	1.99	606.0	11.40	14.60
4	4.11	267.9	5.05	21.90	2.85	642.7	12.10	25.50
5	6.40	94.8	1.79	0.61	4.16	627.1	11.80	35.50
6	8.59	26.3	0.50	5.25	5.35	487.8	9.19	29.80
7	9.99	7.3	0.14	2.42	6.40	331.2	6.24	13.00
8	10.40	1.0	0.02	2.85	7.21	217.0	4.09	1.69
9	9.81	7.9	0.15	7.88	7.62	145.2	2.73	0.18
10	8.49	32.9	0.62	0.00	7.69	104.1	1.96	0.94
11	6.60	37.1	0.70	9.88	7.57	78.2	1.47	0.11
12	4.53	23.3	0.44	8.71	7.14	63.2	1.19	1.22
13	2.77	18.1	0.34	2.32	6.39	43.3	0.82	6.04
14	1.55	25.6	0.48	3.35	5.41	25.9	0.49	8.66
15	0.80	36.7	0.69	1.60	4.34	13.5	0.26	5.06
16	0.39	37.8	0.71	0.39	3.38	6.6	0.12	0.60

^aObtained with the Slater potential curves, transition moments and radial coupling function.

^bObtained with the Gaussian potential curves and transition moments, and the Lorentzian formula for the radial coupling with $W=0.05 a_0$.

^cOnly the term $A_{12} d/dR$ in Eqn (37) is taken into account; B_{12} is neglected.

Table II. Photodissociation cross section for absorption into the uncoupled repulsive diabatic $2^2\Pi_1$ state from the $x^2\Pi(v''=0)$ state.^a

$v' 10^3 f_{0v}^{\text{ad}}$	Slater ^a			Gaussian ^b			Photon energy (eV)	$\sigma^d (10^{-18} \text{ cm}^2)$
	r_v^{ad}	$10^3 k_v^{\text{ad}}$	$10^3 r_v^{\text{ad}}$	r_v^{ad}	$10^3 k_v^{\text{ad}}$	$10^3 r_v^{\text{ad}}$		
0	1.27	582.5	11.00	41.70	2.01	1367.8	25.80	37.90
1	2.47	3227.2	60.80	8.77	4.24	2667.6	50.20	5.93
2	2.71	1005.0	19.00	46.40	0.86	3427.7	6.45	4.16
3	2.06	389.6	7.34	29.70	1.99	606.0	11.40	14.60
4	4.11	267.9	5.05	21.90	2.85	642.7	12.10	25.50
5	6.40	94.8	1.79	0.61	4.16	627.1	11.80	35.50
6	8.59	26.3	0.50	5.25	5.35	487.8	9.19	29.80
7	9.99	7.3	0.14	2.42	6.40	331.2	6.24	13.00
8	10.40	1.0	0.02	2.85	7.21	217.0	4.09	1.69
9	9.81	7.9	0.15	7.88	7.62	145.2	2.73	0.18
10	8.49	32.9	0.62	0.00	7.69	104.1	1.96	0.94
11	6.60	37.1	0.70	9.88	7.57	78.2	1.47	0.11
12	4.53	23.3	0.44	8.71	7.14	63.2	1.19	1.22
13	2.77	18.1	0.34	2.32	6.39	43.3	0.82	6.04
14	1.55	25.6	0.48	3.35	5.41	25.9	0.49	8.66
15	0.80	36.7	0.69	1.60	4.34	13.5	0.26	5.06
16	0.39	37.8	0.71	0.39	3.38	6.6	0.12	0.60

^aObtained with the Gaussian potential curves and transition moment functions. The Lorentzian formula for the radial coupling with $W=0.05 a_0$ was used in the transformation to the diabatic representation.

Table III. The shape parameter $q_{v'}$ and its individual terms in the numerator in a.u. for the vibrational levels v' of the diabatic $^2\pi_2$ state corresponding to three combinations of potential energy curves and couplings*.

v'	$q_{v'}$			$10^3 \bar{D}_2^d$			$10^3 G(E_{v'})$		
	(i)	(iii)	(ii)	(i)	(iii)	(ii)	(i)	(iii)	(ii)
0	-11.05	-14.95	-46.22	-63.6	-90.2	-118.0	-10.6	-34.2	-4.5
1	0.49	-0.49	-1.79	-6.64	20.4	14.4	-0.2	-8.9	5.6
2	-1.70	-0.91	-4.42	-8.35	-9.18	-14.0	-9.4	-11.5	-0.8
3	-32.15	-2.08	2.34	-10.7	-3.94	-8.27	-15.7	-17.9	-3.4
4	4.39	-2.82	2.03	-4.55	-2.81	-5.90	-12.1	-15.5	-3.8
5	2.66	-4.68	1.99	-2.76	-2.43	-4.67	-12.6	-16.3	-5.0
6	1.54	-9.68	2.20	-0.06	-2.53	-4.17	-13.6	-19.5	-6.7
7	0.94	-797.3	2.74	2.59	-2.55	-3.22	-13.7	-23.0	-7.9
8	0.62	10.97	3.79	-3.98	-2.25	-1.74	12.5	-25.0	-7.2
9	0.45	5.19	3.98	-3.44	-1.60	-0.04	10.2	-25.1	-4.5
10	0.42	3.21	-0.72	-1.31	-0.71	1.51	7.8	-24.1	-1.2
11	0.49	2.37	-1.14	1.37	0.23	2.70	6.1	-22.8	1.3
12	0.58	1.66	-0.89	3.32	-1.11	-3.47	4.7	21.7	-2.0
13	0.62	1.34	-0.59	3.74	-1.85	-3.79	3.3	21.0	-1.0
14	0.55	1.19	-0.31	-2.67	-2.36	-3.61	-2.1	20.3	1.0
15	0.30	1.09	-0.13	-0.81	-2.52	-2.90	-1.1	19.1	2.6
16	-0.09	1.04	0.22	0.98	-2.31	-1.79	-0.6	17.3	2.8

* (i) uses the Slater potentials and couplings (ii) uses the Gaussian Potentials and the Lorentzian formula (36a) with $W=0.05 a_0$ with $b=500 a_0^{-2}$.

(iii) uses the Gaussian potentials and the Gaussian formula (36b)

* See footnote to Table III.

Table IV. The factors $V(E_{v'})$ and $\bar{D}_1^d(E_{v'})$ appearing in the denominator of $q_{v'}$ for the vibrational levels v' of the diabatic $^2\pi_2$ state corresponding to three combinations of potential energy curves and couplings*.

v'	$10^3 V(E_{v'})$			$\bar{D}_1^d(E_{v'})$		
	(i)	(ii)	(iii)	(i)	(ii)	(iii)
0	4.38	5.72	1.85	0.49	0.46	0.46
1	-5.90	-8.63	-4.25	0.76	0.96	0.84
2	3.07	5.82	0.89	1.08	1.24	1.20
3	0.18	2.16	-1.05	1.46	1.55	1.51
4	-0.68	1.26	-0.96	1.78	1.64	1.59
5	-0.95	0.72	-0.90	1.94	1.77	1.72
6	-1.31	0.39	-0.85	2.16	1.89	1.85
7	-1.60	0.01	-0.65	2.35	2.04	2.00
8	1.76	-0.36	-0.35	2.50	2.20	2.15
9	1.86	-0.70	-0.16	2.56	2.34	2.30
10	1.96	-1.00	-0.20	2.53	2.46	2.43
11	2.06	-1.19	-0.45	2.37	2.55	2.52
12	2.10	1.53	0.76	2.09	2.58	2.56
13	2.07	1.77	1.01	1.74	2.57	2.55
14	-2.00	1.93	1.09	1.37	2.50	2.49
15	-1.92	2.03	0.94	1.04	2.39	2.39
16	-1.85	2.05	0.66	0.75	2.23	2.24

Table V. Comparison of the shape parameter q_v , obtained from the exact solution of the coupled equations and from the discrete-continuum interaction theory²⁷ for various combinations of potential curves and couplings.*

v'	(i) coupled interaction equations			(ii) coupled interaction equations			(iii) coupled interaction equations		
0	-11.02	-11.05	-15.13	-14.95	-45.94	-46.22	0	-10.0	-9.6
1	0.39	0.49	-0.39	-0.49	-1.78	-1.79	1	12.5	12.9
2	-1.72	-1.70	-0.92	-0.91	-4.43	-4.42	2	-2.8	-2.7
3	-33.35	-32.15	-2.18	-2.08	2.32	2.34	3	2.2	2.1
4	4.36	4.39	-2.98	-2.82	2.01	2.03	4	2.2	2.2
5	2.65	2.66	-5.11	-4.68	1.97	1.99	5	2.4	2.4
6	1.53	1.54	-11.10	-9.68	2.19	2.20	6	2.7	2.8
7	0.94	0.94	83.50	-797.3	2.73	2.74	7	2.9	3.0
8	0.61	0.62	9.29	10.97	3.61	3.79	8	2.7	2.7
9	0.45	0.45	4.83	5.19	2.67	3.98	9	3.6	3.4
10	0.41	0.42	3.04	3.21	-0.24	-0.72	10	2.6	2.6
11	0.47	0.49	2.11	2.37	-1.16	-1.14	11	2.3	2.3
12	0.56	0.58	1.59	1.66	-0.92	-0.89	12	2.0	2.0
13	0.61	0.62	1.30	1.34	-0.62	-0.59	13	1.9	1.9
14	0.66	0.55	1.15	1.19	-0.34	-0.31	14	1.5	1.5
15	0.31	0.30	1.06	1.09	-0.10	-0.13	15	1.2	1.2
16	-0.13	-0.09	1.01	1.04	0.21	0.22	16	0.8	0.8

* See footnotes to Table III.

Table VI. The shift $F(E_{v'})$ in cm^{-1} of the resonance position from the energy $E_{v'}$ of the uncoupled bound diabatic potential $^2\text{H}_2$ vibrational levels v' for various combinations of potential curves and couplings* obtained from the configuration-interaction theory²⁷ and the coupled equation solutions.

v'	(i) coupled interaction equations			(ii) coupled interaction equations			(iii) coupled interaction equations		
0	0	-10.0	-9.6	-46.8	-46.0	-4.3	-4.1	-4.1	-4.1
1	1	12.5	12.9	22.0	22.7	-6.0	-5.8	-5.8	-5.8
2	2	-2.8	-2.7	-4.1	-3.3	-0.2	-0.2	-0.2	-0.2
3	3	2.2	2.1	0.5	0.5	0.6	0.7	0.7	0.7
4	4	2.2	2.2	1.2	1.0	0.6	0.6	0.6	0.6
5	5	2.4	2.4	1.8	1.5	0.7	0.8	0.8	0.8
6	6	2.7	2.8	2.4	1.9	0.9	0.9	0.9	0.9
7	7	2.9	3.0	3.0	2.7	0.8	0.8	0.8	0.8
8	8	2.7	2.8	3.6	3.4	0.4	0.4	0.4	0.4
9	9	2.6	2.6	4.0	3.9	0.2	0.1	0.1	0.1
10	10	2.3	2.3	4.3	4.2	0.0	0.0	0.0	0.0
11	11	2.0	2.0	4.5	4.4	0.0	-0.03	-0.03	-0.03
12	12	1.9	1.9	4.7	4.7	-0.1	-0.1	-0.1	-0.1
13	13	1.5	1.5	4.9	4.9	0.1	0.1	0.1	0.1
14	14	1.2	1.3	5.1	5.1	0.3	0.3	0.3	0.3
15	15	1.0	1.1	5.2	5.0	0.4	0.4	0.4	0.4
16	16	0.7	0.8	4.9	4.8	0.3	0.3	0.3	0.3

* See footnotes to Table III.

References:

1. E.F. van Dishoeck, S.R. Langhoff and A. Dalgarno, *J. Chem. Phys.* 78, 4552(1983); E.F. van Dishoeck and A. Dalgarno, *J. Chem. Phys.* 79, 873(1983); S.R. Langhoff, E.F. van Dishoeck, R. Wetmore, and A. Dalgarno, *J. Chem. Phys.* 77, 1379(1982).
2. G. Wentzel, *Z. Physik* 43, 524(1927); *Physik* z. 29, 321(1928).
3. O.K. Rice, *J. Chem. Phys.* 1, 375(1933).
4. J.N. Murrell and J.M. Taylor, *Mol. Phys.* 16, 609(1969).
5. I.M. Riess and Y. Ben Aryeh, *J. Quant. Spectr. Rad. Trans.* 9, 1463 (1969).
6. F. Fiquet-Payard, *Journ. Chim. Phys.*, (Special Issue), 18, 57(1970).
7. M.S. Child, in Molecular Spectroscopy, Ed. R. F. Barrow, Vol. 2. Chemical Soc. London, Specialist Periodical Report, 1974.
8. P.S. Julienne and M. Krauss, *J. Mol. Spectrosc.* 56, 270(1975).
9. A.L. Roche and J. Tellinghuisen, *Mol. Phys.* 38, 129(1979).
10. M.A.A. Clyne, M.C. Heaven and J. Tellinghuisen, *J. Chem. Phys.* 76, 5341(1976).
11. M.M. Graff, J.T. Nouseley, J. Durup and E. Roueff, *J. Chem. Phys.* 78, 2355(1983).
12. E.E. Nikitin, Chemische Elementarprozesse, ed. H. Hartmann (Springer-Verlag, Berlin, 1968).
13. R.D. Levine, B.R. Johnson and R.D. Bernstein, *J. Chem. Phys.* 50, 1694(1969).
14. M. S. Child, *Mol. Phys.* 32, 1495(1976); M. S. Child and R. Lefebvre, *Mol. Phys.* 34, 979(1979); *Chem. Phys. Lett.* 55, 213(1978).
15. H. Lefebvre-Brion and R. Colin, *J. Mol. Spectrosc.* 65, 33(1977).
16. M.L. Sink, A.D. Bandrauk and R. Lefebvre, *J. Chem. Phys.* 73, 4451(1980).
17. A.D. Bandrauk, G. Turcotte and R. Lefebvre, *J. Chem. Phys.* 76, 225(1982).
18. E.F. van Dishoeck, M.C. van Hemert, A.C. Allison and A. Dalgarno, Abstracts of Contributed Papers, XIII ICPEAC, ed. J. Eichler et al. (Berlin, 1983), p. 48.
19. P.T. Smith, *Phys. Rev.* 179, 111 (1969).
20. M.B. Faist and R.D. Levine, *J. Chem. Phys.* 64, 2953(1976).
21. T.G. Heil, S.E. Butler and A. Dalgarno, *Phys. Rev. A* 23, 1100 (1981).
22. The ALCHEMY systems of programs were developed by P.S. Bagus, B. Liu, A.D. McLean and M. Yoshimine.
23. R. J. Buenker and S. D. Peyerimhoff, *Theoret. Chim. Acta* 35, 33(1974); 39, 217(1975); R. J. Buenker, S. D. Peyerimhoff and W. Butscher, *Mol. Phys.* 35, 771(1978).
24. S.E. Butler, *Phys. Rev. A* 20, 2317(1979).
25. G. Hirsch, P.J. Bruna, R.J. Buenker and S.D. Peyerimhoff, *Chem. Phys.* 45, 335(1980); R.J. Buenker, G. Hirsch, S.D. Peyerimhoff, P.J. Bruna, J. Römeit, M. Bettendorff and C. Petrongolo, Current Aspects of Quantum Chemistry 1981, in: *Studies in Physical and Theoretical Chemistry*, ed. R. Carbo (Elsevier, Amsterdam, 1982), Vol. 21, p. 81.
26. M. Oppenheimer, *J. Chem. Phys.* 57, 3899(1972).
27. U. Fano, *Nuovo cimento* 12, 156(1955); *Phys. Rev.* 124, 1866 (1961); U. Fano and J.W. Cooper, *Phys. Rev. A* 137, 1364(1965).

28. D. R. Bates and R. McCarroll, Proc. Roy. Soc. (Lond.) Ser. A 245, 175(1958).
29. A. D. Bandrauk and J. P. Laplante, J. Chem. Phys. 65, 2602(1976); 65, 2592(1976).
30. E. F. van Dishoeck and A. Dalgarno, Astrophys. J. 277, 576(1984).
31. K. P. Huber and G. Herzberg, Constants of Diatomic Molecules (Van Nostrand Reinhold, Princeton, 1979).
32. G. Herzberg, in Topics in Modern Physics - A Tribute to Edward U. Condon (Colorado Associated University, Boulder, 1971), p. 191.
33. F. J. Comes and G. Schumpe, Z. Naturforsch. 26, 538(1971).
34. M. Rothschild, H. Egger, R. T. Hawkins, H. Pummer and C. K. Rhodes, Chem. Phys. Lett. 72, 404(1980).
35. M. Rothschild, H. Egger, R. T. Hawkins, J. Bokor, H. Pummer, and C. K. Rhodes, Phys. Rev. A 23, 206(1981).
36. M. Glass-Maujean, J. Breton, and P. M. Guyon, Chem. Phys. Lett. 63, 591(1979).
37. B. Pouilly, J. M. Robbe, J. Schamps, and E. Roueff, J. Phys. B 16, 437(1983).
38. R. J. Buenker and S. D. Peyerimhoff, Chem. Phys. Lett. 34, 225(1975).
39. P. S. Julienne, Chem. Phys. Lett. 87, 240(1982).
40. M. S. de Vries, N. J. A. van Veen, M. Hutchinson and A. E. de Vries, Chem. Phys. 51, 159(1980); A. E. de Vries, Comments At. Mol. Phys. 11, 157(1982).
- Fig. 1. The adiabatic $2^2\Pi$ potential energy curves of OH obtained with the Gaussian calculation. The zero of energy is the $v''=0$, $J''=0$ level of the $X^2\Pi$ state.
- Fig. 2. The adiabatic $2^2\Pi - X^2\Pi$ and $3^2\Pi - X^2\Pi$ transition dipole moments as functions of internuclear distance, obtained with the Gaussian calculation. The dashed lines indicate the diabatic $2^2\Pi_1 - X^2\Pi$ and $2^2\Pi_2 - X^2\Pi$ transition moments in the crossing region.
- Fig. 3. The adiabatic radial couplings $\langle \psi(2^2\Pi) | d/dR | \psi(3^2\Pi) \rangle$ as functions of internuclear distance for the Slater and Gaussian calculations (full lines). The short-dashed line indicates the coupling according to the Lorentzian formula, Eqn.(36a), for $W = 0.05 \text{ \AA}$. The long dashed line indicates the coupling according to the Gaussian formula, Eqn.(36b), for $b = 500 \text{ \AA}^{-2}$.
- Fig. 4a. The nuclear wavefunctions $\chi_{1,2}^{\text{ad}}$ resulting from the coupled equations in the adiabatic formulation, obtained with the Slater potential curves and the ab initio radial coupling function at an energy of 4.0 eV above the $2^2\Pi$ state dissociation limit.
- b. The corresponding nuclear wavefunctions $\chi_{1,2}^{\text{d}}$ resulting from the coupled equations in the diabatic formulation.

Fig. 5. The diabatic coupling V_{12}^d as a function of internuclear distance for various calculations. S: obtained with the Slater potential curves and ab initio radial coupling function; GL: obtained with the Gaussian potential curves and the Lorentzian formula for the coupling with $W = 0.05 a_0$; GG: obtained with the Gaussian potential curves and the Gaussian formula for the coupling with $b = 500 a_0^{-2}$.

Fig. 6. The photodissociation cross section for absorption into the coupled excited 2^{π}_1 states from the $X^2\pi(v''=0)$ state.
 a: obtained with the Slater potential curves, transition moments and ab initio radial coupling function.
 b: obtained with the Gaussian potential curves, transition moments and the Lorentzian formula for the radial coupling with $W = 0.05 a_0$. The full arrows indicate the positions of the vibrational levels of the uncoupled bound diabatic curve. The dashed arrows indicate the positions of the first two vibrational levels of the uncoupled bound adiabatic curve.

Fig. 7. Enlargement of the crossing region of the excited 2^{π}_1 potential curves, obtained from the Gaussian calculation. The full lines indicate the adiabatic potential curves and vibrational levels of the $3^2\pi$ state. The dashed lines indicate the diabatic potential curves and vibrational levels of the 2^{π}_1 state.

Fig. 8. The photodissociation cross section for absorption into the coupled excited 2^{π}_1 states from the $X^2\pi(v''=0)$ state, obtained by solving the adiabatic coupled equations for the excited states neglecting the matrix B. The cross section was obtained with the Gaussian potential curves, transition moments and the Lorentzian formula for the radial coupling function with $W = 0.05 a_0$.

Fig. 9. The photodissociation cross section for absorption into the adiabatic $3^2\pi$ vibrational levels from the $X^2\pi(v''=0)$ state, obtained by assuming a Lorentzian lineshape for each line with width r_v^{ad} determined by the Golden rule. The spectrum was obtained with the Gaussian adiabatic potential curves, transition moments, and the Lorentzian formula for the radial coupling with $W = 0.05 a_0$. The dashed line indicates the cross section for absorption into the uncoupled repulsive adiabatic 2^{π}_1 state.

Fig. 10. The photodissociation cross section for absorption into the uncoupled repulsive diabatic 2^{π}_1 curve from the $X^2\pi(v''=0)$ state. S: obtained with the Slater potential curves, transition moments and ab initio radial coupling function; G: obtained with the Gaussian potential for the radial coupling with $W = 0.05 a_0$.

Fig. 11. The photodissociation cross section for absorption into the diabatic excited 2^{π}_1 curves from the $X^2\pi(v''=0)$ state,

obtained by summing the cross section for absorption into the uncoupled diabatic repulsive $^2\Pi_1$ curve and the cross sections for absorption into the diabatic bound $^2\Pi_2$ vibrational levels, assuming a Lorentzian lineshape for each of the lines with width determined by the Golden rule. The Gaussian potential curves and transition moments, and the Lorentzian formula for the coupling with $w = 0.05 a_0$ were adopted.

Fig. 12a-f Enlargements of the resonances corresponding to the vibrational levels $v' = 0-4$ and 10 of the diabatic $^2\Pi_2$ curve, obtained with the Slater potential curves, transition moments and ab initio radial coupling function. The full lines show the profiles resulting from the coupled equations. The crosses (x) indicate the profiles according to the formulation of Fano, Eqn. (40), obtained with the calculated profile parameters and shifts in the diabatic representation. The dashed line indicates the cross section for absorption into the uncoupled diabatic continuum.

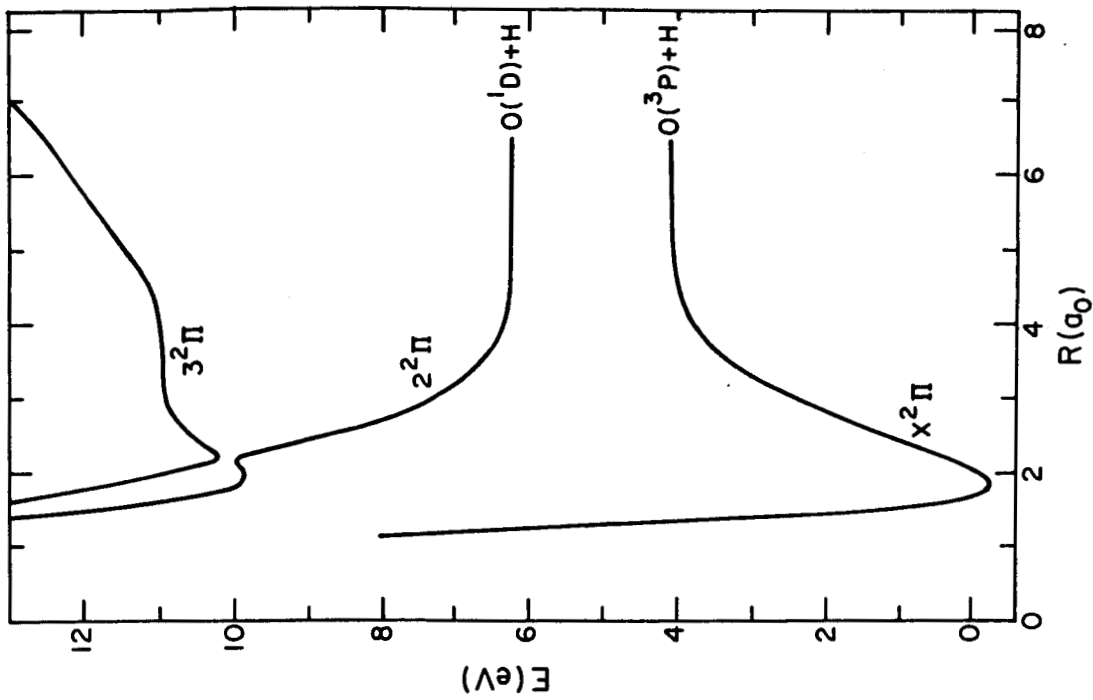


Figure 1

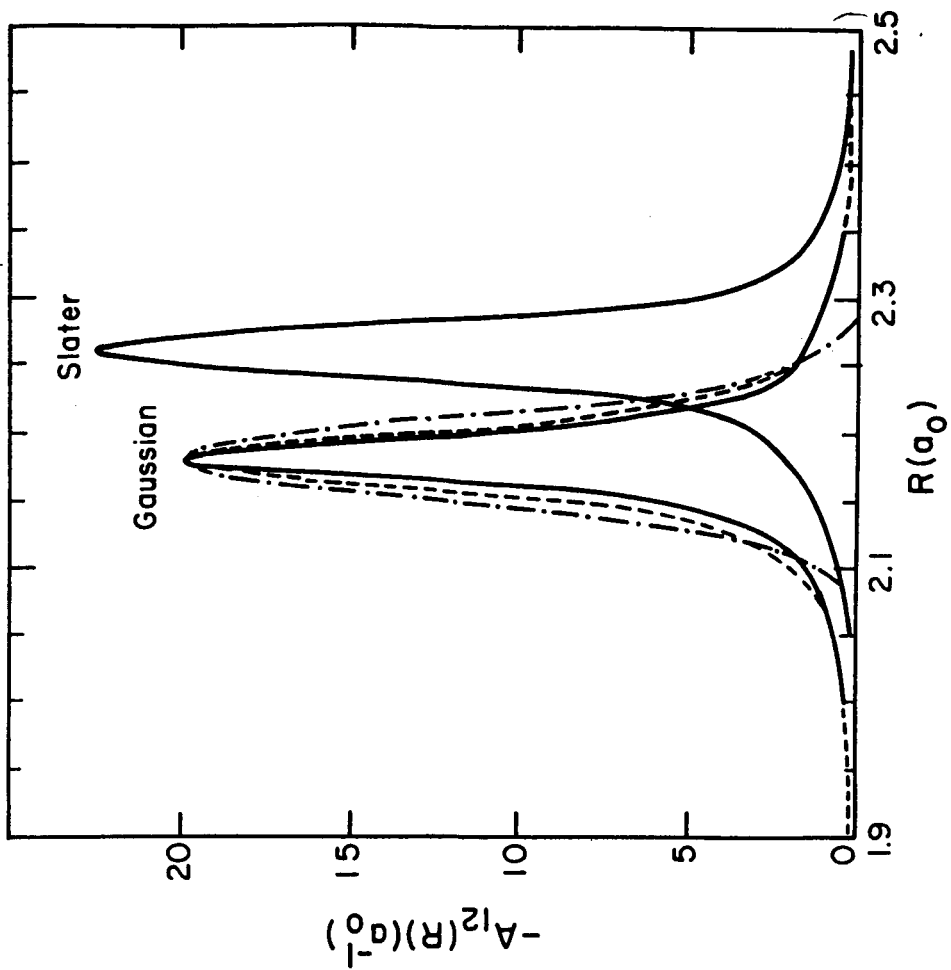


Figure 3

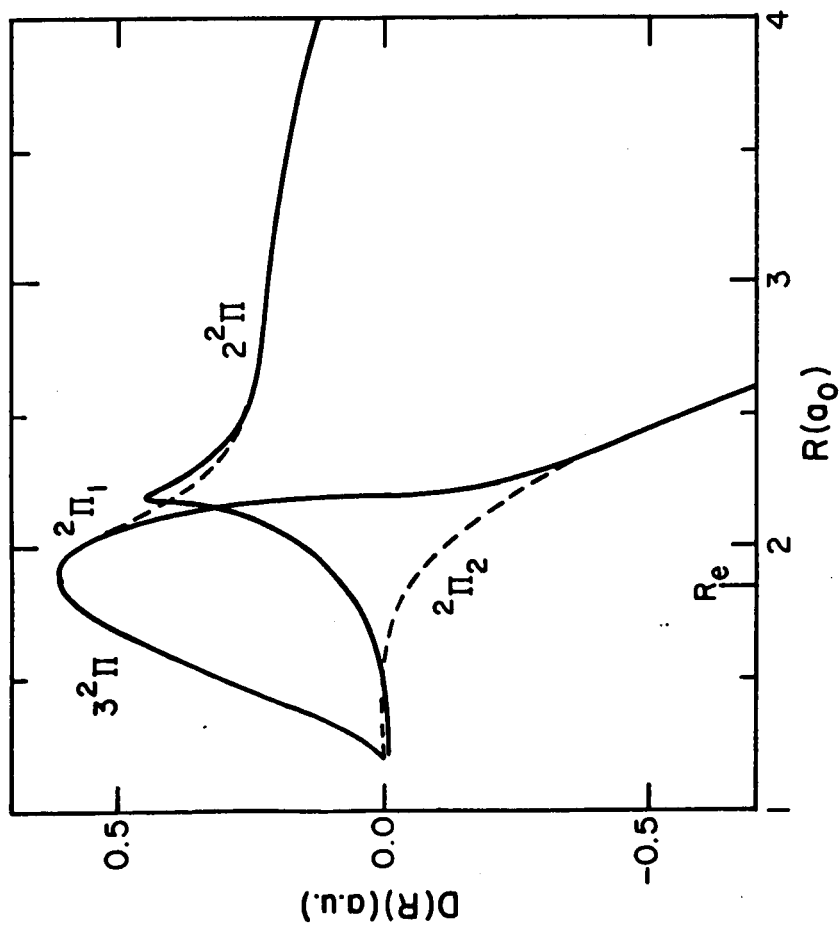


Figure 2

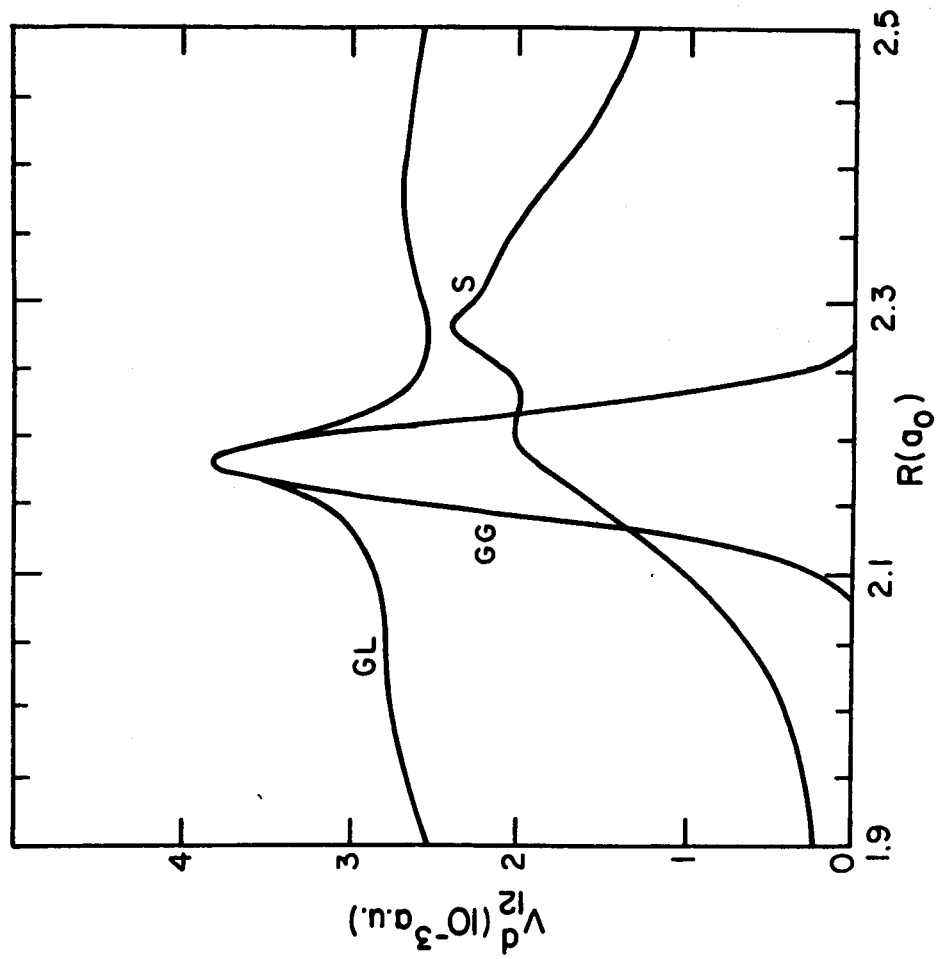


Figure 5

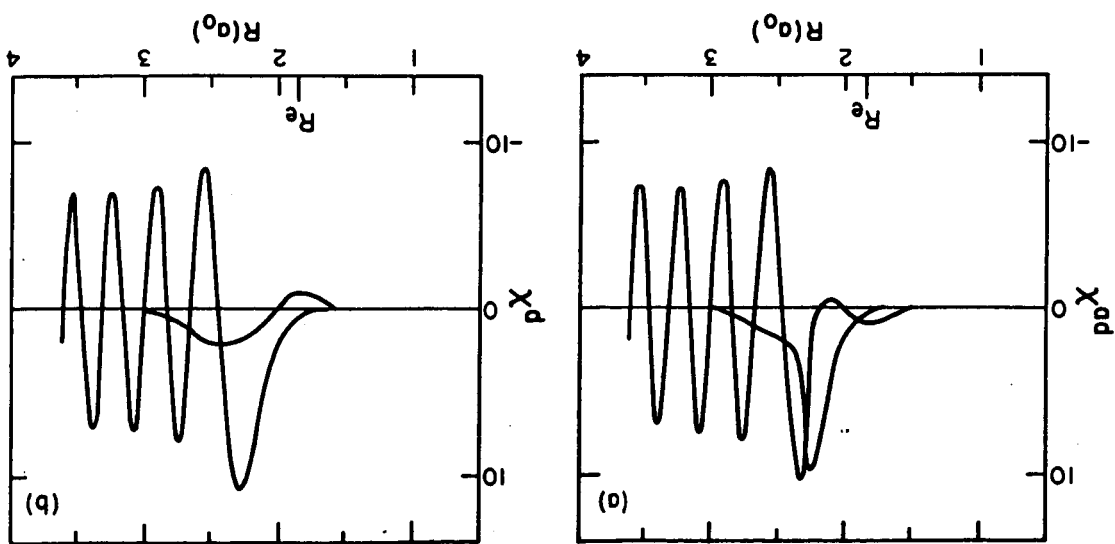


Figure 4

Figure 6b

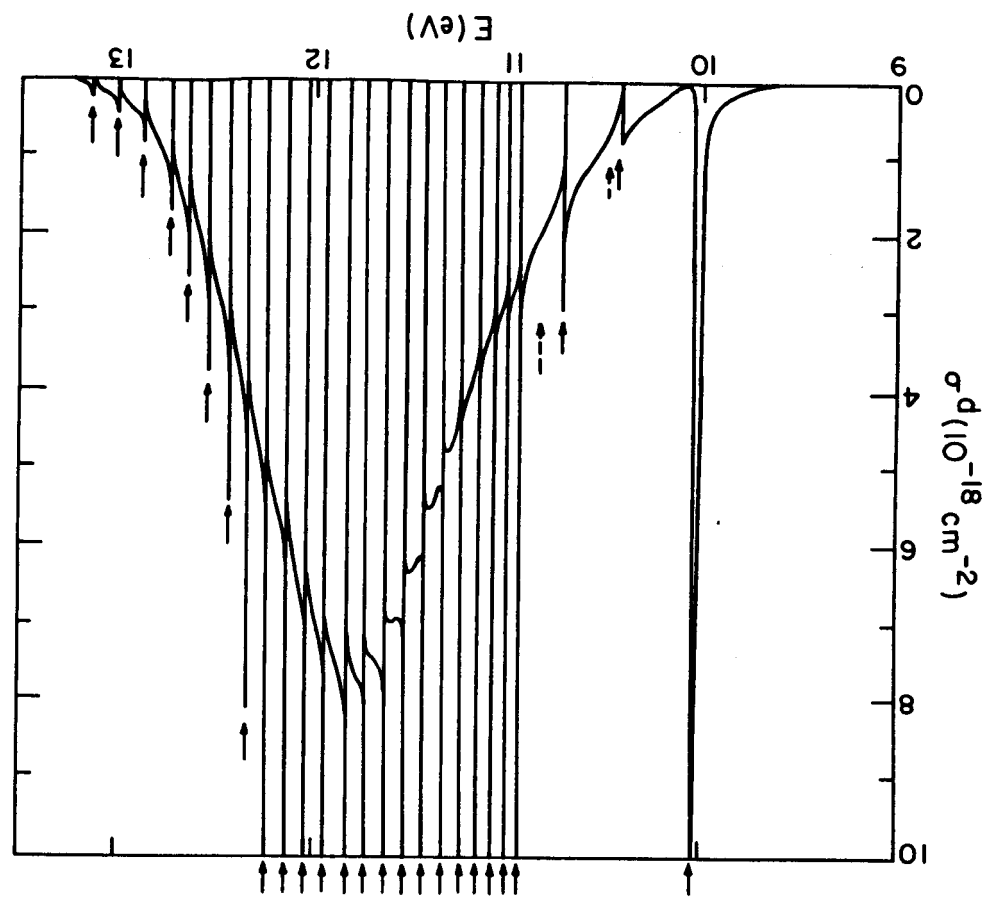
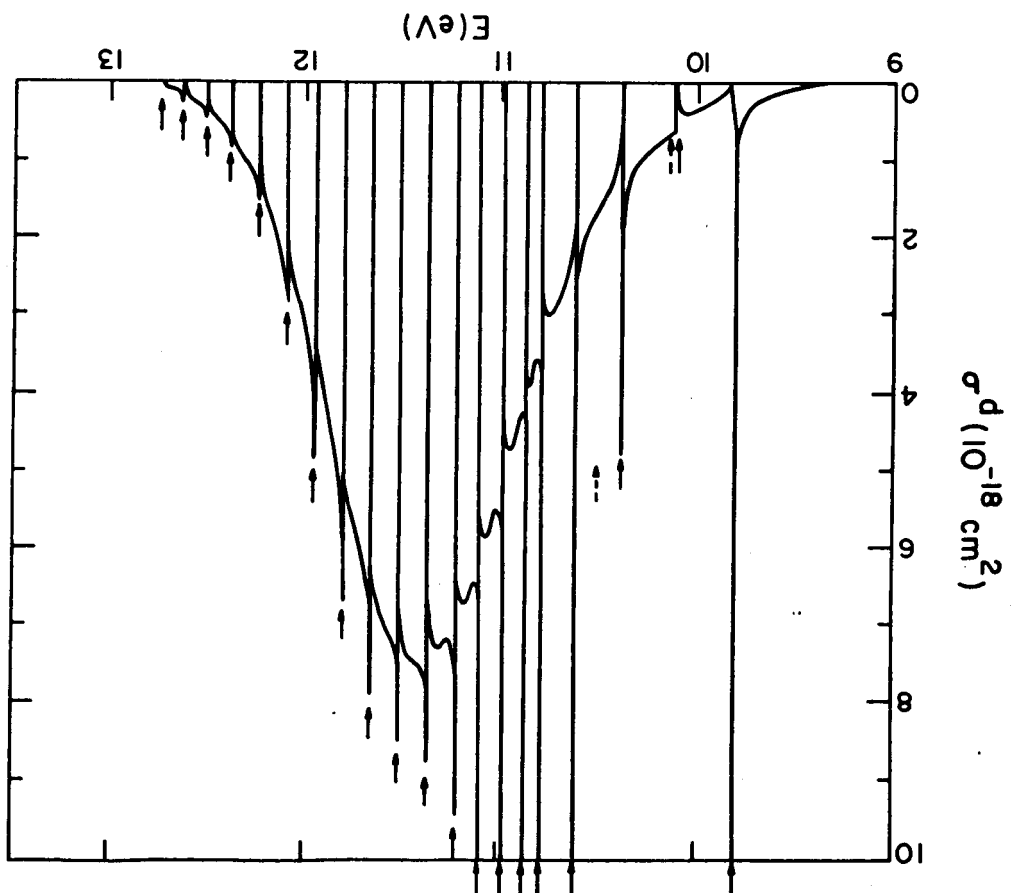


Figure 6a



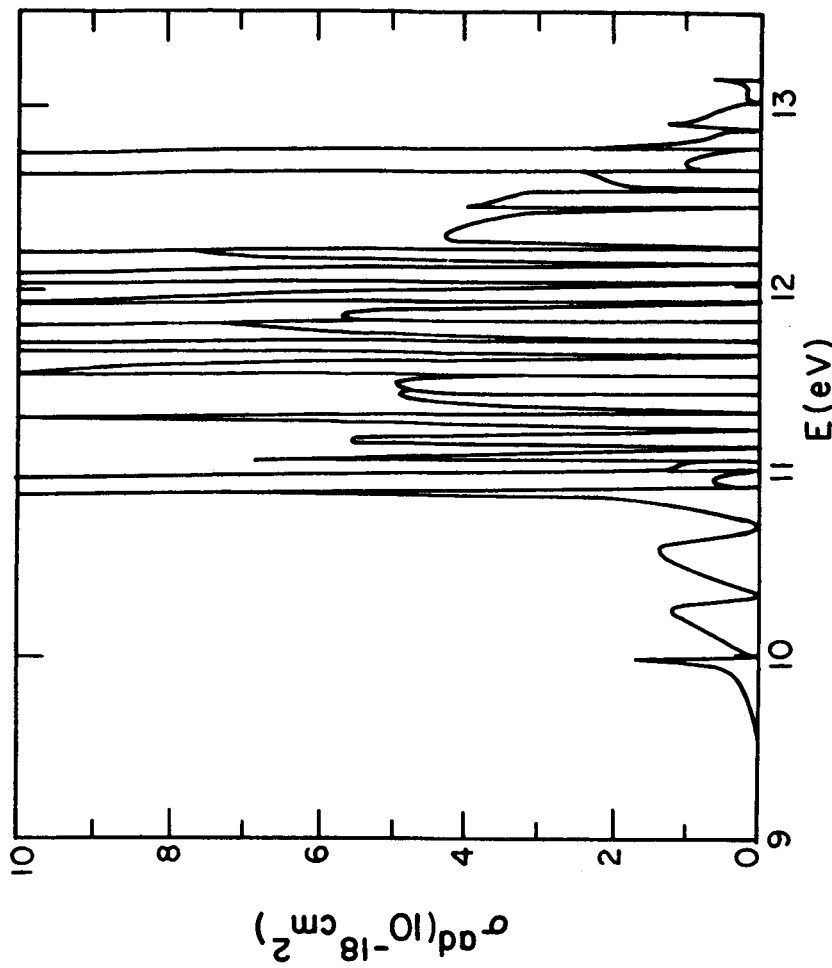


Figure 7

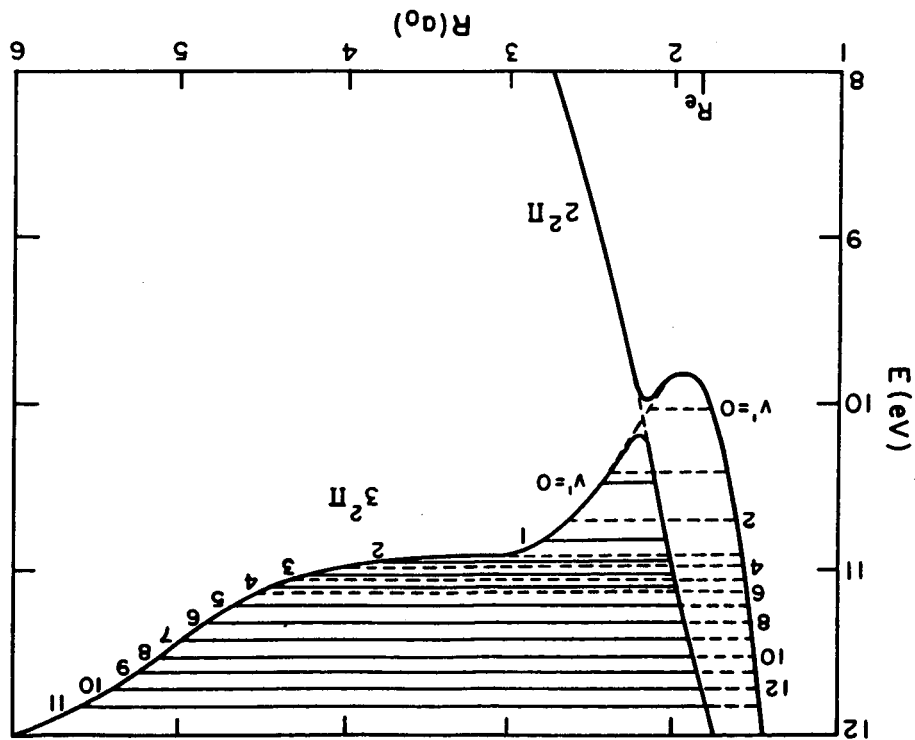


Figure 10

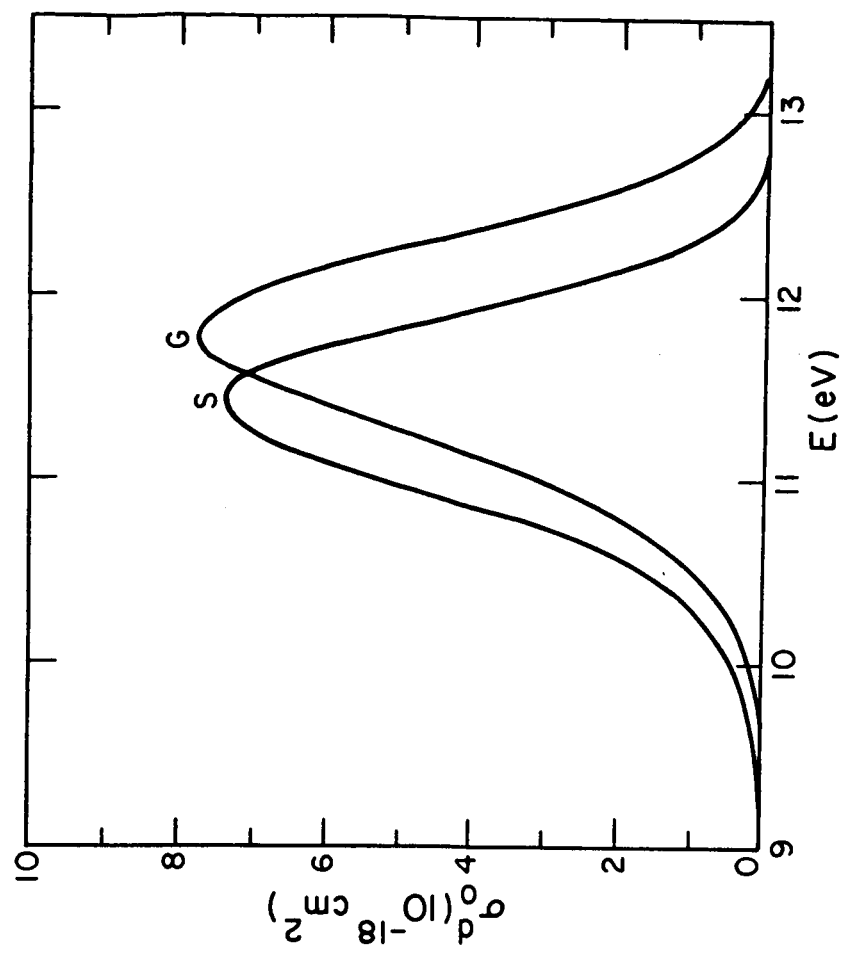


Figure 9

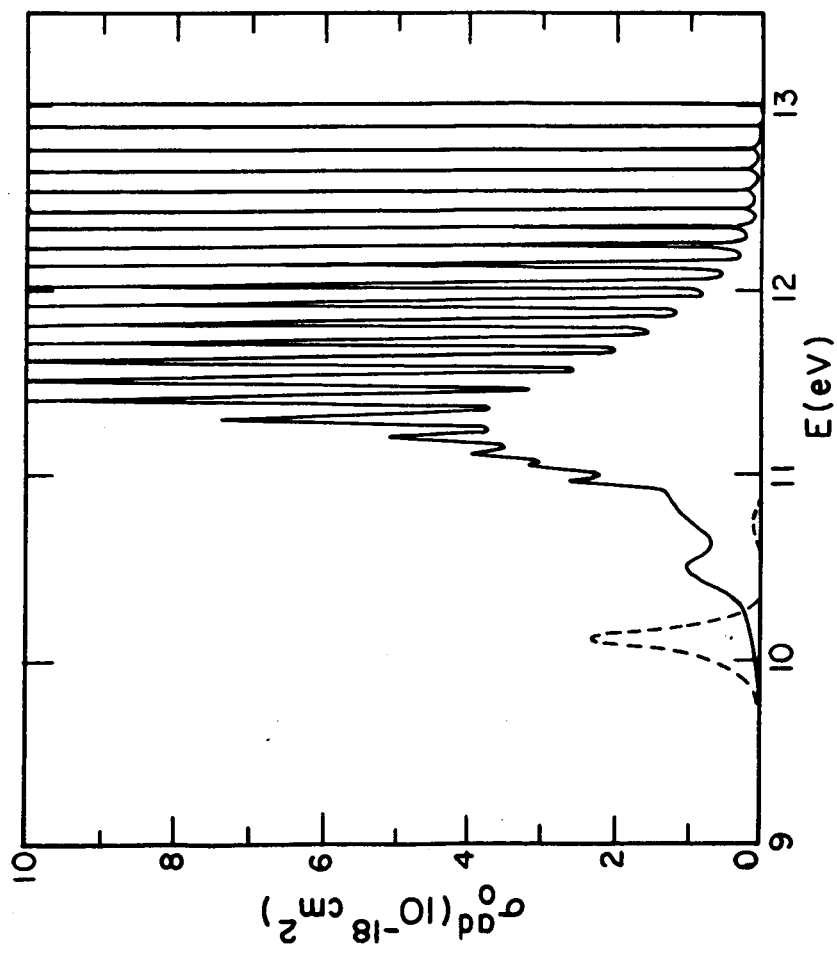


Figure 12

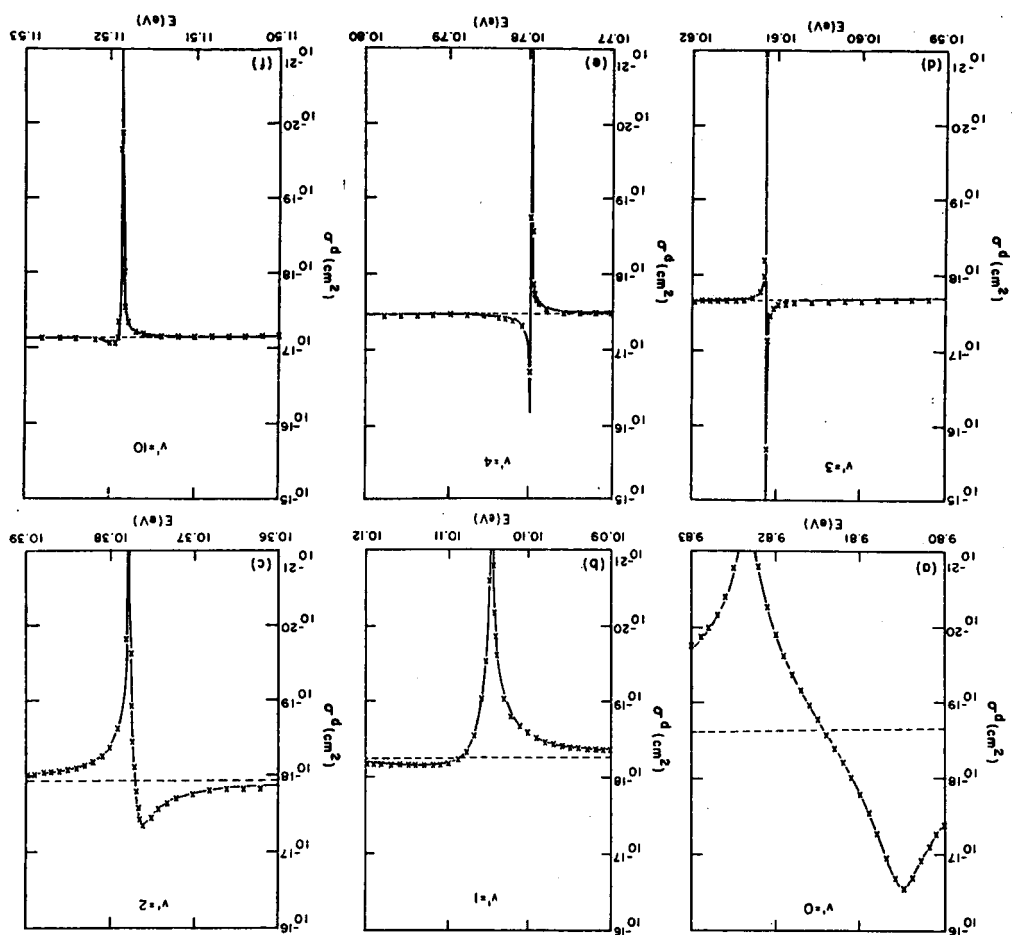


Figure 11

